Computation, Synthesis and NMR Investigations of PROTAC Linker Conformation, Chamaleonicity and their Impacts on the Mode of Action

Hao Lan,[§,†] Oliver Hsia,[Δ] Mark Nakasone,[Δ] Andre Wijaya,[Δ] Alessio Ciulli,[*,Δ] Craig P. Butts,[*,§] & Varinder K. Aggarwal,[*,§]

[§] School of Chemistry, University of Bristol, UK

[Δ] Centre for Targeted Protein Degradation (CeTPD), School of Life Sciences, University of Dundee, Scotland, UK

[†] Present Address: Amphista Therapeutics Ltd, Granta Park, Cambridge, CB21 6GQ, UK

Keywords: PROTAC, Linkerology, Drug Design, Conformational Analysis, Modelling, NMR

ABSTRACT: Linker design is a core task in Proteolysis Targeting Chimera (PROTAC) drug discovery, which influences ternary complex formation for selective target protein degradation as well as physicochemical properties. However, it remains challenging to accurately model the whole landscape towards the formation of ternary complex and understand the influence of linker rigidity/flexibility on each step in the working mechanism of PROTAC. To address this, we revisited a well-established system of the VHL-based BET degrader **MZ1** and also explored the likely ternary complex of **ARV771** with enhanced MD simulation, which explains for the first time the plasticity and selectivity of BET degradation with VHL E3-ligase. Regarding facile conformational change possibly induced by different linkers, the physics-driven modelling of ternary complex was applied to confirm and propose a highly cooperative and potent BET degrader **HL1** which was shown to preferentially degrade BRD4 with a late onset of the hook-effect, similar to **MZ1**. A further novel PROTAC containing a semi-rigid fully sp3 linker, **HL1CON**, was developed to potentially stabilize the **MZ1**-type ternary complex similarly to **HL1** and improve membrane permeability, but also appears to suffer from non-chameleonic hydrophobic collapse in different solutions as well as in VHL binary complexes. This resulted in significant barriers for **HL1CON** to get into cell, bind with either receptor and ultimately form cooperative and productive ternary complex. This study has demonstrated that rational PROTAC linker design is a multi-task object and the rigidification strategy with redundant hydrophobicity does not necessarily benefit degradation activity in our case. The comprehensive modelling of PROTACs in solution, binary complex and ternary complex states based on physics could help us to understand its complicated behaviors and reduce the risk in structure-based linker optimization.

Introduction

Proteolysis targeting chimeras (PROTACs) are molecules which use a linker to conjugate two chemical probes together (**Figure 1**), which separately recruit an E3 ubiquitin ligase and a protein of interest (POI) to form the ternary complex.[1,2] With such proximity, E3 recruits an E2 enzyme to transfer ubiquitin tags onto the target protein in several catalytic rounds before its recognition by the proteasome for induced degradation.[3] Over the past decade, PROTACs have become one of the most promising therapeutic strategies in drug discovery, with abundant cases of intracellular protein degradation having been reported so far and over 20 PROTAC candidates being in clinical development.[1] Among these cases, PROTACs containing a Von Hippel-Lindau (VHL) binding warhead as the E3 handle are commonly used, while the Bromo- and Extra-Terminal domain (BET) family have become standard protein targets to test the potency of PROTAC bearing various linkers and E3 probes, [4–12] and these are the focus of this report.

We have reported the first crystallography of a ternary complex induced by PROTAC **MZ1** (**Figure 1. b**) which consists of **JQ1** (a standard pan-BET ligand), a PEG3 (polyethyleneglycol-3) linker and **VH032** (a standard VHL ligand), which recognises VHL and the BRD4:BD2 domain (part of BRD4 in the BET family) with high cooperativity (**Figure 1. b**).[13,14] This gave potent and preferential degradation of BRD4 in several

cell lines, and downstream Myc depletion as well as cytotoxicity that is sensitive to BET knockout. This was followed by reports of several other cooperative and non-cooperative ternary complex structures from experiment-driven models based on CRBN, cIAP E3-ligase and various POIs apart from Bromodomain families.[9, 10, 12, 23, 24] Arvinas have also reported another pan-BET degrader, **ARV771** (**Figure 1. b**), which possesses a shortened PEG2 linker and showed high degradation potency and efficacy *in vitro* and *in vivo* studies.[7] Further attempts to shorten linker length and folding conformation failed to induce highly potent BET degradation, probably due to an inability to adopt the necessary conformations for ternary complex formation.[6,15,16] In contrast, other degraders bearing longer linkers (e.g., **MZ2** with a PEG4 linker, **Figure 1. b**) still showed potent and BRD4-selective degradation.[5,6] Based on the ternary complex structure of VHL-**MZ1**-BRD4:BRD2, we have developed and reported several other VHL-based BET degraders applying optimisation strategies of macrocyclisation,[17] fluorination,[18] amide-to-ester[19] and trivalency[20] to improve PROTAC binding affinities, induced proximities, and physiochemical properties.

In this work, we applied advanced molecular dynamics simulations to build on the **MZ1** ternary crystallography in solution and propose a likely ternary pose for **ARV771**, which explains the linker-dependent plasticity and selectivity of BRD4:BD2-PROTAC-VHL system. Confirmed by the physical modelling, we have also designed two new BRD4-selective degraders **HL1** (**1**) and **HL1CON** (**2**) (**Figure 1. b**) respectively with flexible hydrophilic and semi-rigid hydrophobic linkers, but which showed contrary behaviours of degradation potency, ternary complex formation, and membrane permeability. With further computation and NMR analysis, redundant hydrophobic collapse of **HL1CON** was identified both in free solutions and when incorporated into VHL binary complexes, which aligned with its lower binding affinities, lower cooperativities and earlier onset of hook-effect compared to **HL1** and **MZ1**. Taken together, these data provide unique insights to understand the PROTAC mechanism of widely reported BRD4 protein degradation based on VHL E3-ligase.

Results

Refinement of MZ1 ternary complex crystallography with enhanced MD simulations

In the **MZ1** ternary complex crystal structure (**Figure 1. b**), the -C-C- and -C-O- dihedral angles of the folded PEG3 linker are not in the low energy conformations that would be expected based on the adjacent C-X bonds *i.e.* the so-called 'gauche effect'.[13,21,22] This discrepancy is likely due to the dominance of strong protein-protein (linker) packing in this single snapshot of the possible ternary structural ensembles.[23] A similar issue has been reported for dBET PROTACs utilising CRBN E3-ligase,[10] in which ternary contact in solution was found to be much more diverse using hydrogen/deuterium exchange mass spectrometry (HDX-MS).[24]

To further explore the conformational behaviour and dynamics of the ternary ensembles, we therefore deployed molecular dynamics simulations with multiple simulated annealing (MSA) (**Figure 2. a**). The relaxation of aliphatic chains to adopt gauche conformations was reported on a timescale of 200 nanoseconds by conventional MD at room temperature,[22] which we confirmed, starting from the crystalline geometry, but with no obvious conformational change of the whole complex (**SI Section_1.1**). To enhance the sampling of complexes, subsequent temperature heating (heating-accelerated pose

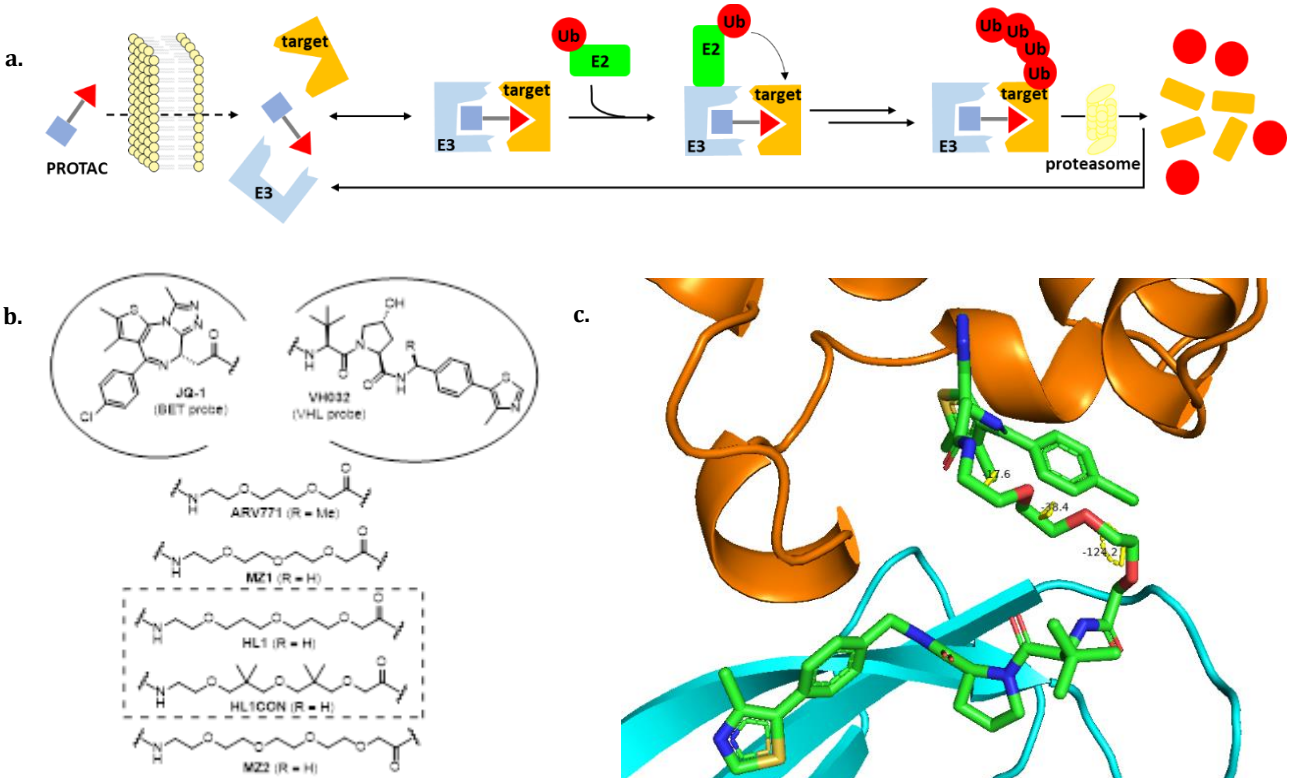

Figure 1. a. The mechanism of PROTAC induced targeted protein degradation. **b**. The structures of **ARV771**, **MZ1** and **MZ2** as representative BET PROTAC degraders from previous reports, together with **HL1** and **HL1CON** designed and investigated in this study. **c.** The ternary crystal structure of **MZ1** (green) with BRD4:BD2 (orange) and VHL (blue) (**PDB: 5T35**). Notably, the -C-C- torsional angles on PEG3 linker in **MZ1** crystal are not folded under ideal gauche states (i.e., 17.6, -38.4 and -124.2 degrees against ~60 degree).

change, HAPOC)[26] and multiple simulated annealing (MD-MSA) were applied (**SI Section_1.2-1.4**), followed by clustering, local descent minimisations and final scoring with Molecular Mechanics Poisson-Boltzmann surface area (MMPBSA) for five equilibrated trajectories. This afforded stable snapshots of the BRD4:BD2-**MZ1**-VHL ternary complex (**Figure 2. b** and **SI Section_2**) which also showed more reasonable gauche conformations of the linker -C-C- bonds. Aligning the VHL components of each minimised snapshot shows that the position of BRD4:BD2 component is rather flexible in the ternary complex ensemble (**Figure 2. b**). Notably, the biaryl moiety of VH032 warhead detached from the HIF binding surface of VHL in one of the minimised snapshots of the ternary complex. This is similar to observations in recent reports of BRD4:BD1-VHL ternary crystal structures for VH032-based PROTAC degraders, which increases our confidence that simulations could reproduce experimental behaviours.[27,28]

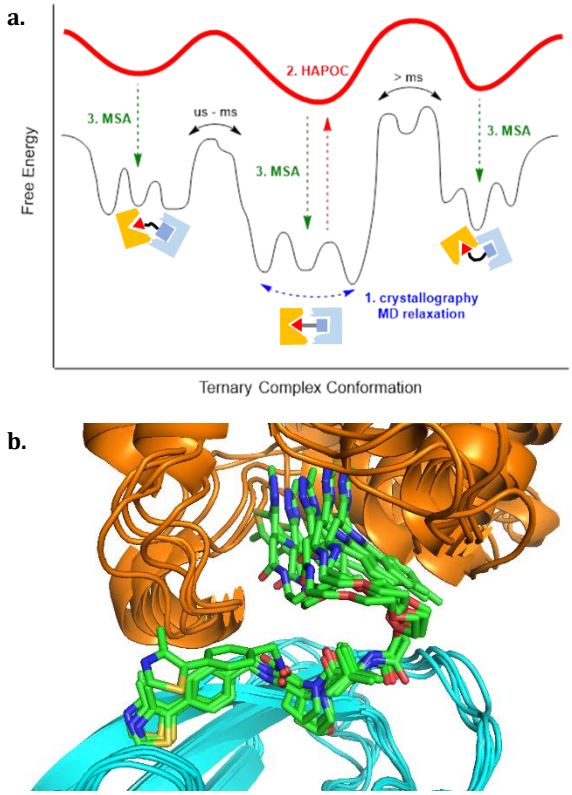

Figure 2. a. The scheme of multiple simulated annealing (MSA) after classic 200 ns MD relaxation and HAPOC for enhanced sampling of ternary complex poses (OPLS-AA, BRD4:BD2 backbone restrained). **b.** The top 5 stable ternary complex snapshots for **MZ1** (VHL-aligned, blue) based on MD-MSA sampling, minimisations and scoring with MMPBSA.

The linker-dependent ternary complex plasticity

The MD-MSA approach also captured the event of significant conformational transition (upper, **Figure 3. a**) and revealed a cluster with new contacts between the BRD4:BD2 αZ' moiety and VHL β-domain L7 loop (lower purple, **Figure 3. a**) while the original interaction between BRD4:BD2 αZ'' region and VHL β-domain S4 sheet was lost. According to MMPBSA scoring of overall stability (**SI Section_2**), this new cluster appears to be a transient local minimum for **MZ1** ternary complexes. The identification of such a conformational transition in solution demonstrates that our MD-MSA approach based on crystallography could provide additional insight compared to those widely reported (semi)rigid protein-protein docking workflows derived from Monte-Carlo approaches (e.g., MOE, RosettaDock, PRosettaC, FRODOCK and 'half-linker' FFT) for efficient search of ternary complex poses often starting from random poses with separate restraints by linker conformational space.[29–34]

In this new MD-derived cluster, the PEG3 linker adopted more extended conformations (**Figure 3. a**) rather than the collapsed state found by crystallography and conventional MD relaxations (**Figure 2. b**). These ternary poses also showed different protein-protein interfaces that might be more suitable for incorporating **ARV771** with its shorter linker,[7] which is also suggested by our recent biophysical and mutation studies showing that **ARV771** should have native poses different from **MZ1**.[19,35] To test this, we replaced **MZ1** in the local minimum of ternary complex with **ARV771** and ran five replicates of 200 ns simulation (**SI Section_3**). Most trajectories converged to structures which maintained the new contact between BRD4:BD2 and VHL, and all poses had very similar PROTAC conformations to each other (lower left, **Figure 3. b**). Further MMPBSA scoring (**SI Section_4**) confirmed the high stability of main clusters which are almost identical in geometry. Moreover, all dihedral angles on the PPG2 linker of **ARV771** were seen to relax into reasonable conformational states in the ternary complex ensemble. For example, in the most stable snapshot scored by MMPBSA (lower, **Figure 3. b**), the PPG2 linker conformation adopted an antiperiplanar-gauche-antiperiplanar-antiperiplanar (*ap-g-ap-ap)* conformation for dihedral angles of the central propylene bonds from the JQ1 to VH032 end of the linker. This model is consistent with a stable conformation predicted by *ab initio* calculations of the parent 1,3-dimethoxypropane fragment.[36,37]

In addition to the difference in conformation between the **MZ1** and **ARV771** linkers (**Figure 3. c**), the VHL-based alignment of different states also suggested a possible repulsion between the extra methyl group in **ARV771** ('R' in **Figure 1. b**) and the backbone amide of LEU-385 on BRD4:BD2. Nevertheless, our previous study indicated that the **ARV771** analogue without such methyl substitution on **VH032** still showed pan-BET degradation activities,[19] indicating that it is the difference of linker rather than the 'R' group on **VH032** warhead that affects the ternary complex plasticity of two PROTACs in this case.

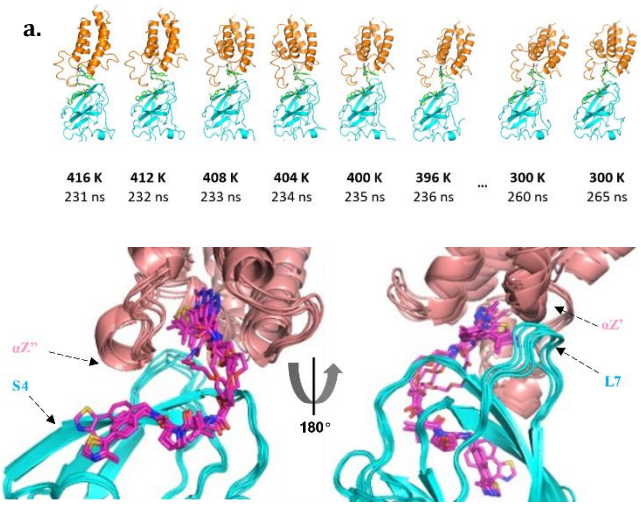

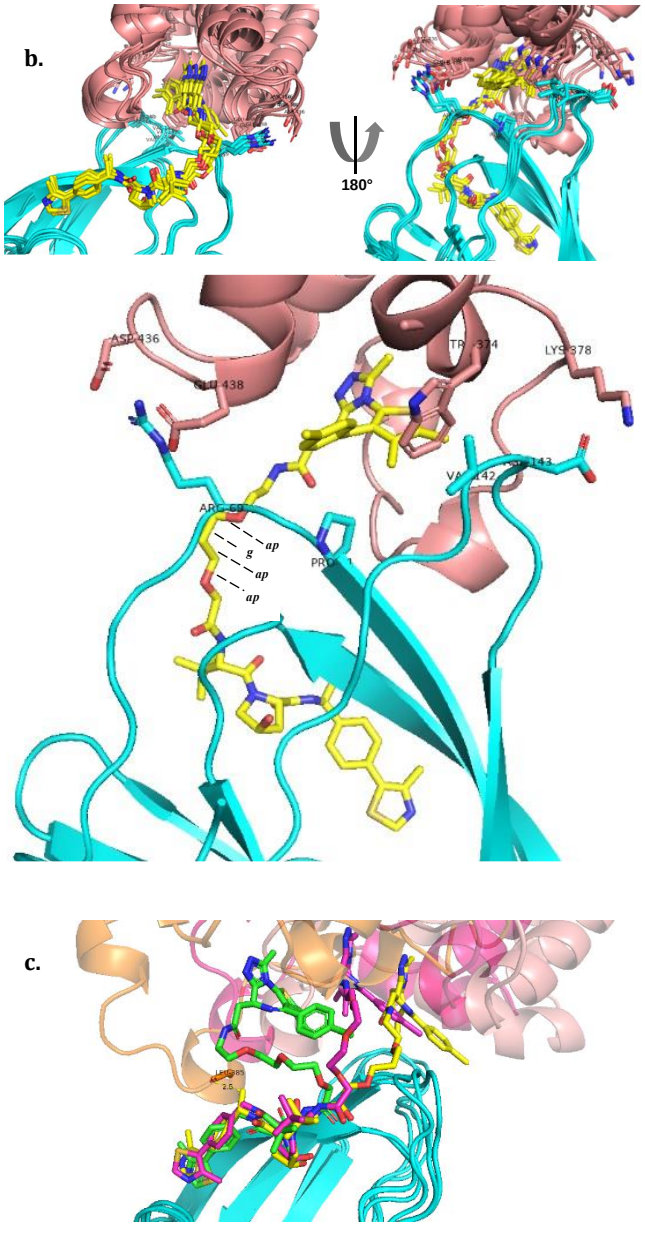

Figure 3. a. A local minimum of **MZ1** ternary complex was sampled by MD-MSA starting from crystallography. **b.** The ternary complex for **ARV771** was modelled and relaxed from **MZ1** local minima (5*200 ns simulations). Five most stable poses for **ARV771** scored by MMPBSA are highly aligned (upper); The best scored snapshot for **ARV771** was shown with reasonable linker conformation and induced PPIs (lower). **c.** The overlay of crystal structure of **MZ1** (green stick with BRD4:BD2 in orange), **MZ1** local minima (purple stick with BRD4:BD2 in magenta) and **ARV771** (yellow stick with BRD4:BD2 in pink) in their ternary complexes with VHL (blue).

The theoretical pose of ARV771 supported by its pan-BET degradation selectivity

In the most stable complex modelled for **ARV771** (**Figure 3. b and SI Section_5**), we observed a new hydrophobic interaction between W374 (BRD4:BD2 αZ') and V142 (VHL β-domain L7) as well as the formation of two new salt bridges: K378 (BRD4:BD2 ZA loop) with D143 (VHL β-domain L7) and R69 (VHL β-domain L1) with D436 (BRD4:BD2 αC). Compared to the **MZ1** native poses (upper, **Figure 4**), the two salt-bridges between R107/R108 (VHL S4) and E383 (BRD4:BD2 αZ'') were lost while the salt-bridge between R69 and E438 is preserved (lower, **Figure 3. b**). Notably, R107 also forms new electrostatic interactions with the thiazole moiety in poses for **ARV771** (lower, **Figure 4**), which we attribute to the lost interaction with E383 (BRD4:BD2 αZ'') from **MZ1** native poses (upper, **Figure 4**). We hypothesise, the extra methyl group ('R') on **ARV771**, also facilitate this new interaction for better VHL binding affinity and indirectly contributes to distinct ternary complex formation by avoiding a steric clash with BRD4:BD2 in the original position led by **MZ1** (**Figure 3 c**).[19]

The theoretical model for **ARV771** is validated by BET sequence comparison. The BD2 domains in both BRD2 and BRD3 share corresponding residues required for the interactions with VHL according to the model (marked in green in **Figure 4**). This could explain the pan-BET degradation activities observed for **ARV771**. Moreover, the **ARV771** ternary model has the P71 (VHL β-domain S1, **Figure 3. b**) shielded under the JQ1 warhead, which is different from the original hydrophobic interaction between P71 and W374 as indicated from **MZ1** ternary crystallography and MD-MSA refinements (**SI Section_5**). This is in line with our recent study focusing on P71I mutation,[35] which reduced BRD4 degradation activity of **MZ1** but not **ARV771**.

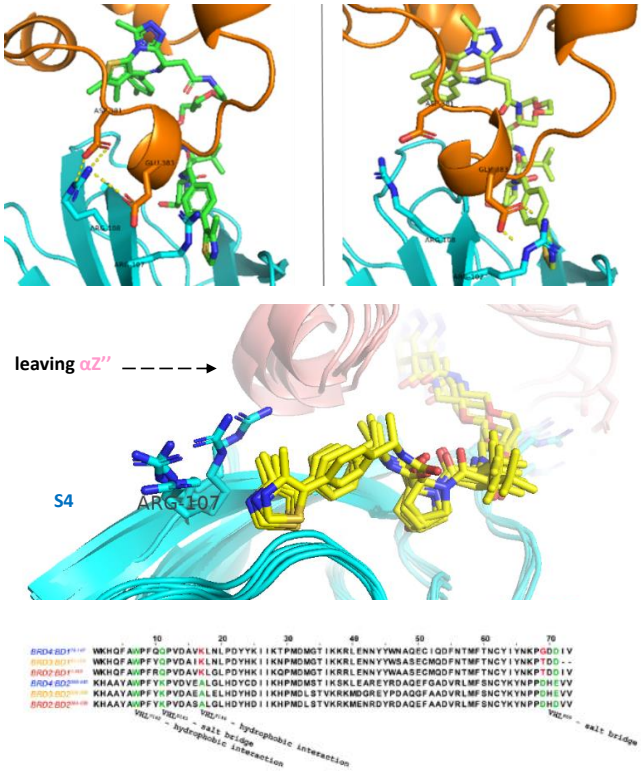

Figure 4. The salt-bridge interactions between BRD4:BD2 αZ'' and VHL β-domain S4, indicated by **MZ1** crystallography (upper left) and a snapshot from MD-MSA minimisations (upper right). Such contact between BRD4:BD2 αZ'' and VHL S4 does not exist in the simulated poses for **ARV771** (lower). We highlighted all specific protein-protein interactions in the theoretical pose for BRD4:BD2 (magenta)-**ARV771** (yellow)-VHL (blue). The homology sequence alignment based on such model explained pan-BET degradation selectivity for **ARV771**.

https://doi.org/10.26434/chemrxiv-2024-5dbnb **ORCID:** https://orcid.org/0000-0001-9671-9009

MZ2 ternary complex dissociation insight from MD-MSA

We next explored MD-MSA minimisations for the ternary complex formed by alternative PROTAC **MZ2** with PEG4 linker, again starting from the protein positions in crystallographic geometry for **MZ1** ternary complex.[25] Herein, we observed facile dissociation of the **VH032** warhead from the corresponding HIF pocket on VHL β-domain, while its JQ1 warhead remained bound to the BRD4:BD2 domain (**SI Section_2**). We suggest that this simulated behaviour observed for **MZ2**, which is supported by ternary complex formation experiments reported from our group previously,[13,14] is due to the labile collapse of long PEG4 linker onto BRD4:BD2 surface. This contrasts with the **MZ1** ternary complex which remained associated in our MD-MSA workflow, although two recent theoretical studies respectively based on steered MD (SMD)[22] and τ-Random Accelerated MD (τ-RAMD)[55] suggested there is a possibility for **MZ1** to stay on the surface of VHL E3-ligase after BRD4:BD2 dissociation even though BRD4:BD2 is rather tightly bound by the highly affinitive **JQ1** warhead. Given the different stabilities between ternary complexes of **MZ1** and **MZ2** according to computational modelling, we were interested in rationally designing and synthesising novel linkers for optimizing VHL-based BET PROTACs with improved proximity, permeability and potency for BRD4-selective degradation. Furthermore, enhanced simulations of ternary complex would be helpful to check the possibility of conformational change induced by different linkers in design process, as warned by cases between **ARV771** and **MZ1**.

Structure-guided linker optimisation and rigidification with precise conformational control

To reduce strain in the ternary complex due to high energy conformations of the bound PROTAC linker, we elongated the linker in **MZ1** from PEG3 to PPG3 to afford the design of **HL1** (**Figure 5 a**). The PPG3 chain was expected to reduce the strained gauche effects of -C-C- dihedrals in PEG3 linker, and this hypothesis was supported by MD-MSA simulation and MMPBSA scoring of **HL1** linker-modified ternary complex after relaxation, which suggested a stronger induced PPIs contribution rather than PROTAC binding contribution to the overall stability of system (**Figure 5 b**).

Notably, the PPG3 linker was simulated to adopt *ap* states for all its -C-O- dihedrals according to minimised MD snapshots of **HL1** ternary complex with OPLS force-field (**Figure 6 c** and **SI Section_2**), while its -C-C- dihedrals adopted *g* states. This was in line with previous conformational analysis of parent 1,3-dimethoxypropane, of which *ab initio* calculations suggested these are the optimal arrangements in free-state.[36,37] We also incorporated β-gem-dimethyl substitutions into the PPG3 linker, giving rise to the design of **HL1CON**, to explore the effect of rigidifying linker conformation (**design details in SI Section_6**). Under MD-MSA simulations and minimizations, **HL1CON** was computed to retain the stability of the **MZ1**-type ternary complex similarly to **HL1** (**Figure 5 b**), although the modelling also suggested that the intramolecular hydrophobic collapse of **HL1CON** ligand were observed in its complex (**Figure 5 c**). This phenomenon even appeared at the HAPOC heating stage prior to annealing relaxations and minimisations (**Figure 5 d**), according to the RMSD analysis of ligand aligned in corresponding complex.

Besides ligand collapse, no other new pose of ternary complex for **HL1** and **HL1CON** was sampled by our MD-MSA approach starting from linker-modified **MZ1** crystallography. This contrasted with the case of **MZ1** which displayed a different pose

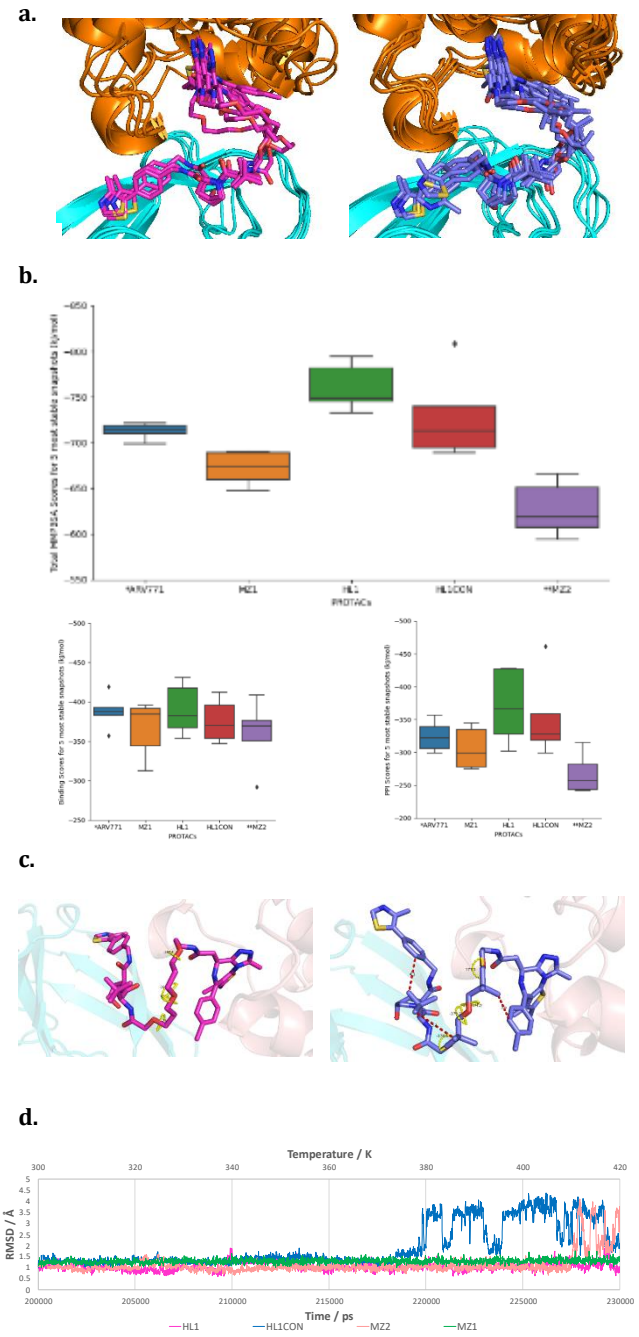

Figure 5 a. The structures of **HL1** and **HL1CON** were designed by using PPG3 linkers with proper length between PEG3 of **MZ1** and PEG4 of **MZ2**. **b.** The scores of top 5 stable snapshots of ternary complex for **HL1** and **HL1CON**, predicted by MD-MSA minimization and MMPBSA, in comparison with **MZ1**, **MZ2** and **ARV771**. ***ARV771** adopt poses different from other PROTACs. ****MZ2** scores exclude cases of dissociation. **c.** The best scored snapshot for **HL1** (left) and **HL1CON** (right) in corresponding ternary complex, both of which approach **MZ1**-type. In addition to reasonable dihedral angles in both cases (yellow), **HL1CON** ligand also showed internal hydrophobic collapse (close contacts highlighted by red dashed lines) when fold within the complex. **d.** According to ligand RMSD analysis, the hydrophobic collapse of **HL1CON** in its complex was found to arise even at the heating stage prior to annealing.

that was more suitable for **ARV771**. We therefore hypothesise that **HL1** and **HL1CON** with linkers longer than the PEG3 in **MZ1** could take on a productive pose for BRD4:BD2 recruitment and BRD4 selective degradation among BET family.

Linker synthesis and conformational analysis

To test our predictions made by simulation, **HL1** and **HL1CON** were taken forward to synthesis (**SI Section_7**), based on four linker models **3**, **5**, **7** and **9** (**Figure 6 a**). We investigated the native conformations of these linkers in solution using $^{3}J_{CH}$ NMR scalar coupling constants around the corresponding dihedral angles in both chloroform and DMSO (**SI Section_7**).[38,39] Pleasingly, these experimental data reproduced computed ensembles for these molecules based on unrestrained Monte-Carlo conformational search (MMFFs/GBSA, MacroModel), extensive DFT minimisations (B3LYP(D3)/6-311+G**/IEFPCM, **Figure 6 a**) and subsequent GIAO calculations (wb97xd/6-311G**, **Figure 6 b**).[40–43,65] The population analysis of the PPG3 chains in these NMR-validated conformational ensembles confirmed the design principles of **HL1CON**, with its -C-O- dihedral angles biased toward *ap* or *ac* states by the steric effect of β-gem-dimethyl substitutions (**Figure 6 b and SI Section_8**). Meanwhile, for each -C-C- dihedral angle regardless of β-gem-dimethyl substitution, the *g* state was slightly preferred over the *ap* state, probably attributed to a balance between hyperconjugation/anomeric effects and electrostatic repulsion between oxygens (**SI Section_9**). Notably, several intramolecular hydrogen bonding (IMHB), C-H π-stacking and lipophilic interactions between the linker termini were observed by DFT minimisations in solution (**Figure 6 a**). This could indicate the 'chameleonicity' of PROTACs potentially based on these linkers. Further MD simulation and potential of mean-force (PMF) analysis in explicit water (OPLS-AA with TIP3P) suggested the rotation of -C-C- dihedral is also kinetically inhibited by the β-gem-dimethyl substitution, as designed for **HL1CON** (**SI Section_10**). Taken together, this conformational analysis of the isolated linkers supported **HL1CON**, with β-gem-dimethyl substitutions on the PPG3 linker, as an attractive design to rigidify **HL1** and was ideally to stabilize the bioactive conformation in the ternary complex with BRD4:BD2 and VHL.

Contrary BRD4 degradation activities, binding affinities, cooperativities and caco-2 permeabilities between HL1 and HL1CON

The amide conjugation of JQ1 and VH032 warheads to linkers **7** and **9** afforded **HL1** and **HL1CON** (**SI Section_11**). Together with **MZ1** and **MZ2**, these BET-targeting PROTACs were analysed using western blotting in HeLa and HEK293 cells (**Figure 7 a**). **HL1** (BRD4(s) DC_{50} = 6.7-11 nM) was found to be a

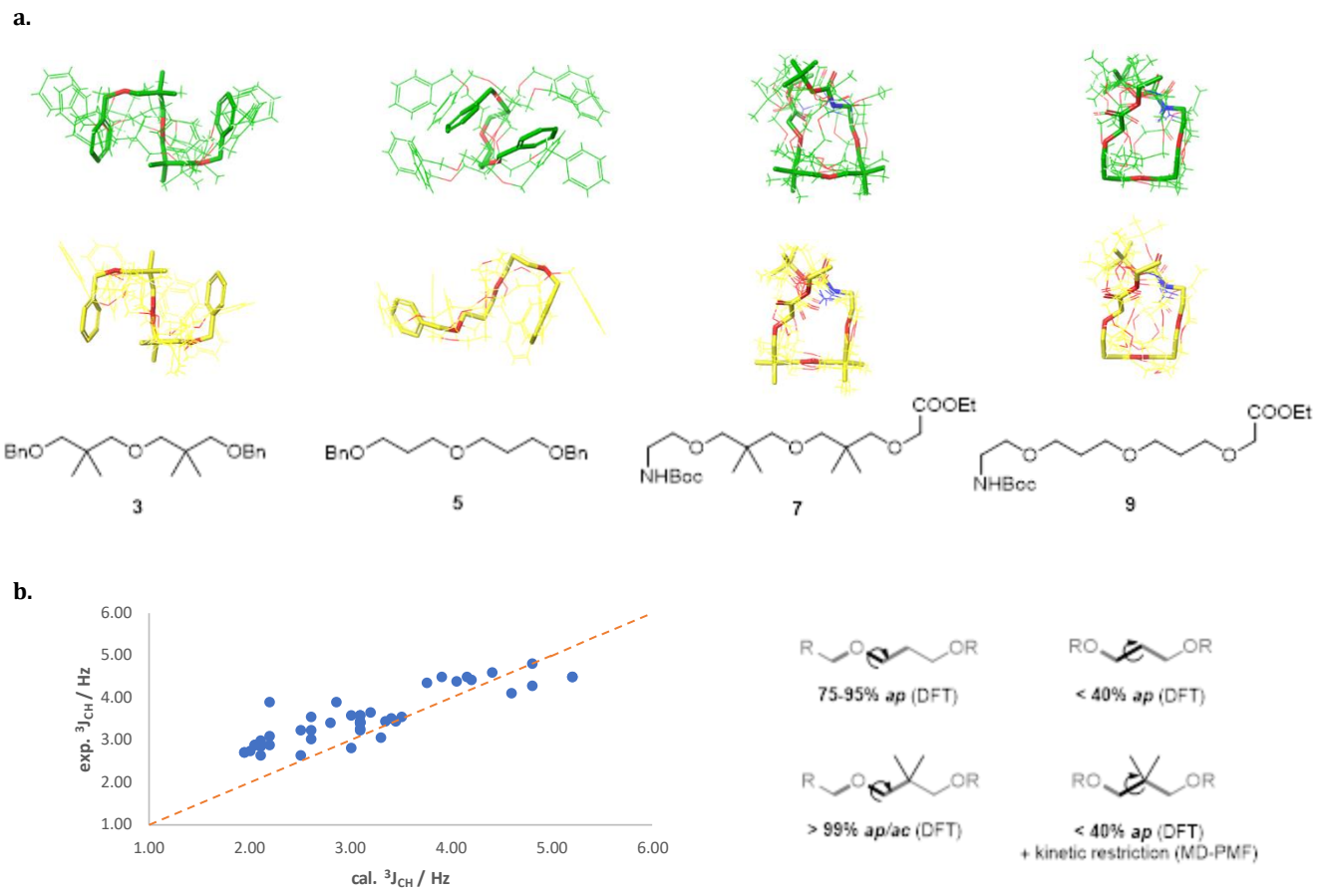

Figure 6. a. The conformational ensemble for **3**, **5**, **7** and **9** respectively in chloroform (green, global minimum in stick) and DMSO (yellow, global minimum in stick). **b.** The scalar coupling constants $^{3}J_{CH}$ extracted from IPAP-HSQMBC were used to validate dihedral angles in MCMM-DFT computational ensembles of four PPG3 chains in solution (B3LYP(D3)/6-311+G**/IEFPCM). The modelling and NMR analysis confirmed stronger *ap* conformational control on the -C-O- dihedral by the β-gem-dimethyl substitution and weak *g* preference for the -C-C- dihedrals in both substituted and unsubstituted substrates. These solution-state linker analysis are in line with bioactive conformations of **HL1** and **HL1CON** predicted by MD-MSA minimisations.

similarly potent BET degrader to **MZ1** (BRD4(s) DC_{50} = 10-22 nM) while **HL1CON** showed a lower potency (BRD4(s) DC_{50} = 60-100 nM). **HL1CON** also showed the earliest onset '*hook-effect*' at 10 uM among the four candidates (**SI Section_12**) - the concentration-activity phenomenon of a three-body system that manifests via the competitive formation of intermediate binary complexes intracellularly when PROTAC concentrations substantially exceed the two protein concentrations.[44,45] All four VHL-based degraders showed moderate selectivity of BRD4 over BRD2 and BRD3 in the BET family (**Figure 7 a**), in line with the observation from MD-MSA modelling showing that **HL1** and **HL1CON** have comparable binding modes to **MZ1** and **MZ2**, but differ from the non-selective **ARV771**. Furthermore, HiBiT-BRD4 degradation in HEK293 cells (upper, **Figure 7 b**) confirmed the trend of degradation potency (**HL1** = **MZ1** > **MZ2** >> **HL1CON**). Although **HL1CON** (HiBiT BRD4 DC_{50} = 441 nM) is not as potent as three other degraders, good efficacy (D_{max} > 95%) could still be achieved at relatively high concentration. The BET-sensitive MV-4-11 cell viability for the four degraders (lower, **Figure 7 b**) found that **HL1** showed superior cytotoxicity (EC_{50} = 0.9 nM, E_{max} = 97%) compared to **MZ1** (EC_{50} = 0.7 nM, E_{max} = 94%) while both **MZ2** and **HL1CON** induce far less apoptosis except at high dose.

The following AlphaLISA (αlisa) assessment of binding affinities to the BRD4:BD2 receptor (**Figure 7 c and SI Section_13**)[46] found that **MZ1** was strongest (K_d = 9.3 nM), followed by **MZ2** and **HL1** (K_d = 56.1 nM and 57 nM respectively), whereas **HL1CON** (K_d = 549 nM) showed the weakest binding affinity. We then measured their binary binding affinities with the E3-ligase using fluorescence polarisation (FP) assay (**SI section 13**).[14,19] Once again **HL1** (VCB K_d = 248 nM) and **MZ2** (VCB K_d = 223 nM) showed modest decay compared to **MZ1** (VCB K_d = 95 nM), with **HL1CON** (VCB K_d = 1679 nM) having a significantly lower binding affinity.

The efficiencies in ternary complex formation (IC_{50} and α = binary IC_{50} / ternary IC_{50}, **Figure 7 d**) for each PROTAC showed that **HL1** has highly positive cooperativity (α = 41 from αlisa, 52 from FP) comparable to **MZ1** (α = 32 from αlisa, 39 from FP) and **MZ2** (α = 27 from αlisa, 31 from FP), while **HL1CON** showed the lowest cooperativity (α = 14 from αlisa , 3 from FP) in the series. This ranking of cooperativities measured from αLISA and FP assays is consistent with cellular degradation potency (i.e., **HL1** ~ **MZ1** > **MZ2** > **HL1CON**), suggesting the importance of PROTAC-mediated recognition between BRD4:BD2 and VHL E3-ligase for efficient BRD4 degradation in the system of this study.

a.

Cell Lines	BET family	MZ1 DC_{50} (nM)	HL1 DC_{50} (nM)	HL1CON DC_{50} (nM)	MZ2 DC_{50} (nM)
HEK293 (N=2)	BRD2	49	41	131	171
	BRD3	46	20	96	93
	BRD4(S)	10	6.7	60	20
HeLa (N=1)	BRD2	39	63	118	365
	BRD3	82	49	111	640
	BRD4(S)	22	11	100	89

b.

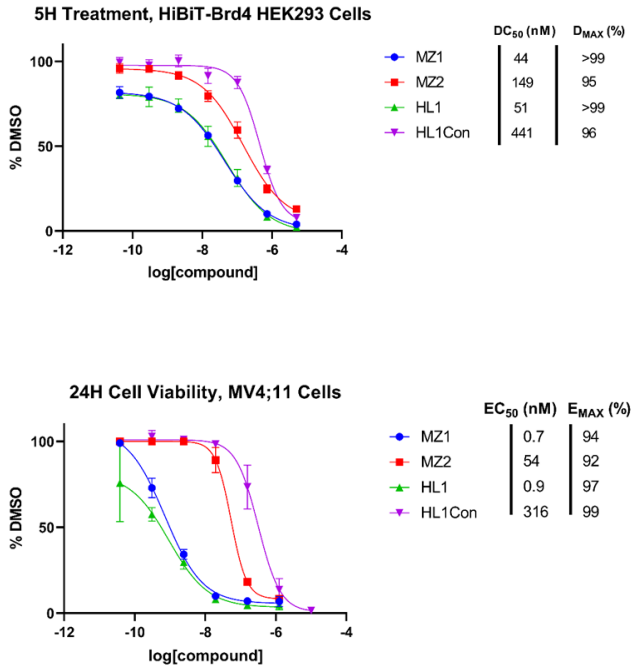

c.

	BRD4:BD2 (αLisa) binary K_d / nM	*VCB (FP) binary K_d / nM*
MZ1	9	95
HL1	57	248
HL1CON	549	1679
MZ2	56	223

d.

	4BD2 (αLisa) IC_{50}/nM	*4BD2 +VCB IC_{50}/nM*	*α*	*VCB (FP) IC_{50}/nM*	*VCB +4BD2 IC_{50}/nM*	*α*
MZ1	93	2.9	32	570	15	39
HL1	287	7.2	41	9400	180	52
HL1CON	3712	257	14	11000	4000	3
MZ2	168	6.3	27	4400	140	31

Figure 7. a. The BET degradation selectivity and potency of **MZ1**, **HL1**, **HL1CON** and **MZ2** (western-blot analysis, 6 hours). **b.** The analysis of endogenously HiBiT tagged BRD4 degradation in HEK293 cells (up) (N = 2). The MV4-11 cytotoxicity of four BRD4-selective PROTACs (down) (N = 2). **c.** The PROTAC binary binding affinities with BRD4:BD2 from AlphaLisa assay and with VCB from FP assay. **d.** The binary and ternary binding efficiency (IC_{50}) and derived cooperativities. *The measurement of ternary K_d < 2 nM was found highly sensitive to assay conditions.

Interestingly, for strong binding PROTACs **HL1**, **MZ1** and **MZ2**, there is a good correlation between the ΔH_{PPI} term of total MMPBSA scores of MD-MSA minimised ternary complex snapshots and the cooperativities measured from αLisa/FP experiments (**Figure 8**). This is in line with the report from Li et al.,[25] highlighting the importance of induced protein-protein interactions for PROTAC cooperativity and ternary complex stability. Moreover, according to the analysis of heating stage in MD-MSA workflow (**Figure 5. d**), **HL1CON** had both the least cooperativity and the lowest temperature (< 380 K) that could tolerate the ligand collapse and departure from the native ternary complex, which support the previous HAPOD study.[26]

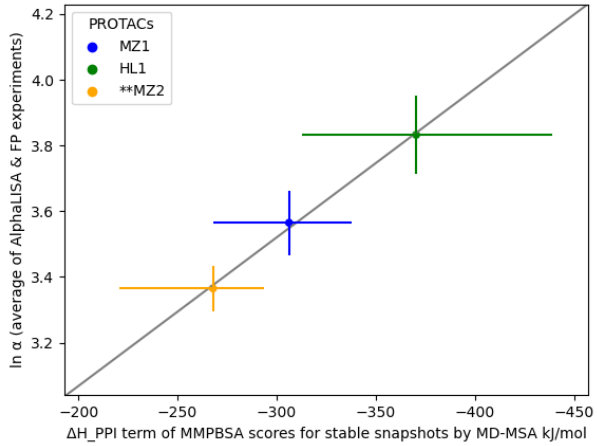

Figure 8. The correlation between experimental cooperativities and MMPBSA-calculated ΔH_{PPI} scores of MD-MSA minimised stable snapshots for strong binding PROTACs under similar poses of ternary complex. **MZ2 scores exclude those cases of dissociation.

We then characterized chromologD, solubility and bi-directional caco-2 cell permeabilities for **MZ1**, **HL1** and **HL1CON** (**Table 9 and SI Section_15**). Both **MZ1** and **HL1** displayed positive physicochemical properties (chromologD ~ 3.25; medium to high kinetic solubilities around 30-60; detectable bi-directional permeability coefficient (P_{app}) despite relatively high efflux ratio (ER > 12)).[49] Pleasingly, **HL1** bearing the PPG3 linker showed slightly improved P_{app} and ER compared to **MZ1** bearing PEG3, suggesting the limited increase in number of methylene units can benefit cell permeability while not impairing solubility in this case. Unfortunately, further increasing hydrophobic character appears to be detrimental, with **HL1CON** having high lipophilicity (cLogD = 4.73), poor kinetic solubility (< 10) and a permeability that was below the experimental limit of detection.

Hence, **HL1**'s comparable BRD4 selective degradation efficiency to **MZ1** might be attributed to its better permeability combined with equally high cooperativity for the BD2 domain of BRD4. For **HL1CON** with redundant hydrophobicity against permeability, its early onset of the hook-effect seems to be less relevant to the permeability since **HL1CON** could not penetrate and build-up intracellular concentration efficiently,[19] but more correlated with its intrinsic low cooperativity (i.e., binary complex formation is competitive with the formation of ternary complex).

Table 9. The summary of *in vitro* DMPK parameters for MZ1, HL1 and HL1CON with different linkers.

	cLogD[a]	Kinetic solubility[b]	Caco-2 A2B (Rec.)[c]	Caco-2 B2A (Rec.)[c]	ER[d]
MZ1	3.17	68.08	0.37 (93%)	6.93 (92%)	18.9
HL1	3.38	30.69	0.58 (79%)	7.35 (106%)	12.7
HL1 CON	4.73	7.83	*BLD (14%)	0.13 (20%)	N/A

[a]chromatographic logD7.4, determined by HPLC method. [b] 1 h read at 620 nm for solubilities in uM DPBS pH=7.4. [c]Permeability/10-6 cms-1 (recovery ratio) [d]Efflux ratio. *BLD = Below limit of detection.

HL1CON suffers from severe hydrophobic collapse in all solutions which against 'chameleonicity'

To further rationalise the lower binding affinities, cooperativities and permeabilities of **HL1CON**, we examined the preferred conformational space of PROTACs in solution. Kihiberg and co-workers have applied the NMR-based NAMFIS approach for conformational elucidations of several cell permeable PROTACs beyond rule of five (bRo5) which are able to fold chameleonically depending on solvation environments.[50,51] They suggested that the PROTAC permeability benefit from IMHBs and reduced polar surface area (PSA) under a compact conformation also indicated by low radius of gyration (R_{gyr}). This was followed by the hydrophobic collapse study of **MZ1** from AstraZeneca according to NMR and MD simulations in explicit solvents.[22]

Following previous linker conformational analysis, we then explored the conformational space of **MZ1**, **HL1** and **HL1CON** with unrestrained Monte-Carlo search (OPLS/GBSA, MacroModel) and affordable DFT-level energy minimisations (ωB97MD3bj/def2-TZVP//B3LYPD3/6-31G*/PCM). The low-energy ensembles of conformers were validated by experimental rotating-frame nuclear Overhauser enhancement (rOe), based on methods previously reported in our group.[41–43,52–54] These studies were conducted in chloroform (ε = 4.8) and DMSO (ε = 47) to approximate polarities of lipid bilayer interior (ε = 3.0) and aqueous solution (ε = 80) respectively.[50]

For both **HL1** and **HL1CON**, solution ensembles were predicted to be dominated by a small number of clustered and minimized geometries (**Figure 10 a** in chloroform; **b** in DMSO) and they were supported by comparison of their Boltzmann-averaged rOe-distances with the experimental rOe measurements (**Figure 10 c**). Frustratingly, severe overlap in the NMR spectra of **MZ1** prevented the extraction of sufficient rOe data for validating its computed ensembles, hence **MZ1** folding was not concluded in this study.

The analysis of conformational ensembles for **HL1CON** indicated it has generally more IMHBs, lower PSA and lower R_{gyr} than **HL1** in both chloroform and DMSO solutions (**SI Section_15 & Section_16**). We also noticed that **HL1CON** showed more rOe between its **JQ1** and **VH032** warheads in relatively polar DMSO solution, suggesting it might suffer from hydrophobic collapse likewise in aqueous solution. This was tested by further conformational sampling and DFT minimisations in

water, which showed the same global minimum conformation as calculated in DMSO (**Figure 10 d** & **SI Section_16**). Due to insolubility in aqueous solutions, experimental validation was obtained by the addition of 25% water to DMSO solutions of **HL1CON.** This showed several rOe among hydrophobic ᵗButyl and methyl groups (upper, **Figure 10 d**). Specifically, the rOe signal ***C*** (5.5 Å) between two terminal methyl groups on the 2D structure of **HL1CON** was clearly seen in the mixture solution (**SI Section_16**). In contrast, theoretical ensembles of **HL1** in both pure DMSO and pure water showed less compact folding (mean 3D-PSA > 160 Å, R_{gyr} up to 6.0, **SI Section_16**), suggesting **HL1** is prone to have more diverse conformations than those highly populated collapse states for **HL1CON**. The addition of water into DMSO mixtures also enhances hydrophobic collapse, shown from the reduction of rOe distance in each PROTAC case (**Figure 10 d** & **SI Section_16**).

Hence, we hypothesize that strong lipophilic collapse should negatively influences PROTAC cell permeability, and it does not appear to support 'chameleonicity' theory whereby the ability to adopt multiple conformations would be expected to allow both membrane penetration and aqueous solubility. Instead, for **HL1CON** as the example in this study, its intensive self-collapse does not drive such molecule to get into water-phase or leave membrane, which was indicated by the low-recovery ratios from bi-directional caco-2 assay (**Table 9**).

a.

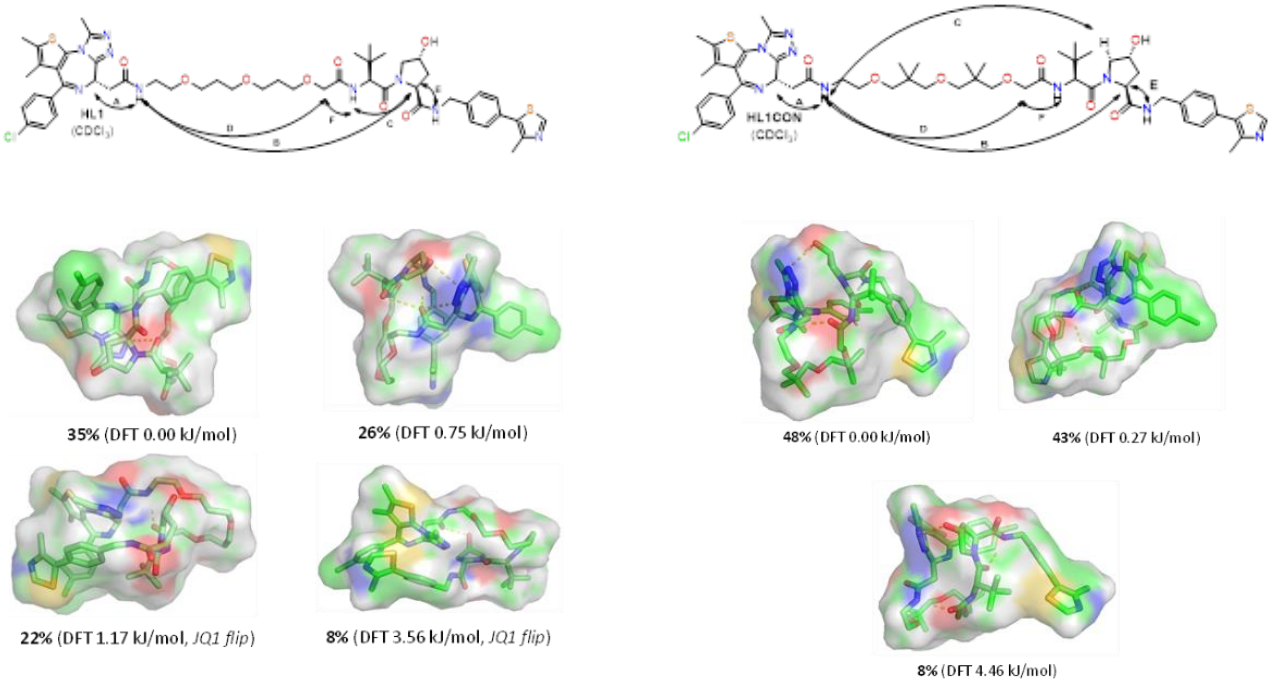

b.

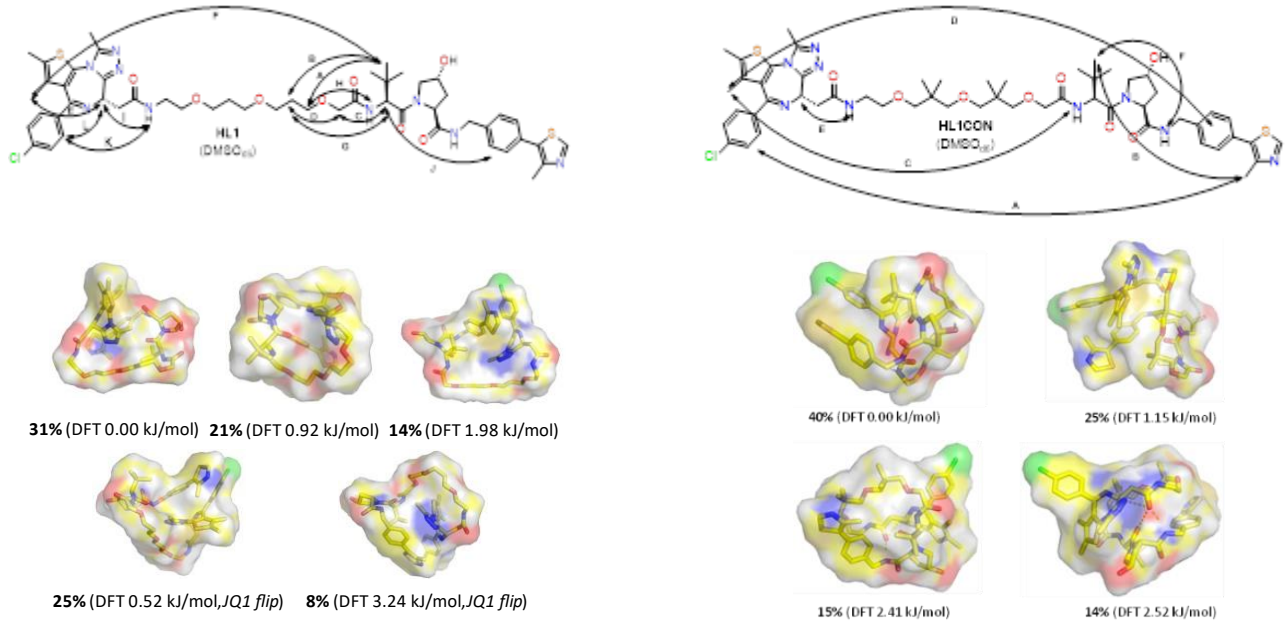

c.

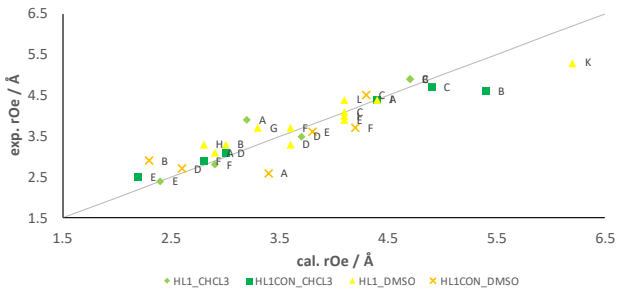

d.

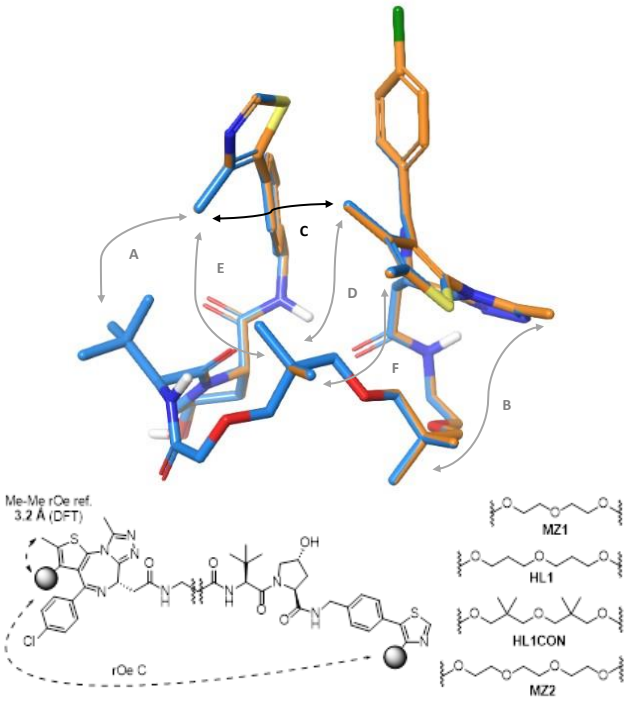

PROTAC	rOe C	D_2O	$DMSO_{d6}$
MZ1	5.6 Å	65%	35%
MZ1	5.8 Å	50%	50%
HL1	5.8 Å	50%	50%
HL1	6.4 Å	25%	75%
HL1CON	**5.5 Å**	**25%**	**75%**
MZ2	5.7 Å	50%	50%

Figure 10. a. The calculated MCMM-DFT solution ensembles for both **HL1** and **HL1CON** respectively in chloroform; **b**. in DMSO. (ωB97MD3BJ/def2-TZVP//B3LYPD3/6-31G*/PCM). **c.** The Boltzmann-averaged rOe distances calculated for above ensembles were validated by experiments (2D-ROESY, 500 MHz). **d.** The global minimum conformation calculated for **HL1CON** in water is identical to DMSO state, labelled with main experimental rOe observed in the mixture. Further 1D-selective-rOe measurements in DMSO/water mixtures supported such specific hydrophobic collapse state for **HL1CON.** This behaviour is different from other PROTACs with hydrophilic and flexible linkers.

Having computed the preferred equilibrium minima states for the hydrophilic and permeable **HL1** with MC-DFT modelling, we explored its kinetic behaviors using MD in explicit water (**Figure 11 & SI Section_16**) and compared it to **MZ1**. During each unbiased 2 us simulation at 300 K (OPLS with initial geometries from DFT-calculated global minima), the **MZ1** with shorter PEG3 linker remained in relatively discrete U-shaped local minima for hundreds of nanoseconds at a time, which reproduce the phenomenon reported by a previous simulation based on the GAFF force-field.[22] In contrast, the **HL1** bearing longer PPG3 linker, rapidly oscillated on a short timescale (< 10 ns) among many distinct states after an initial period of equilibration. We hypothesize the kinetic behavior of **MZ1** in solution may facilitate its binary binding process under less entropic penalty as reported in other PROTAC systems,[62] with the converse true of **HL1**. This is supported by further simulation results of the more flexible **MZ2** (**SI Section_16**). Notably, we observed frequent transitions of opened conformations (R_{gyr} > 0.8 nm) for these flexible and hydrophilic PROTACs in water, indicating possible pathways toward POI/E3 engagement feasibly.

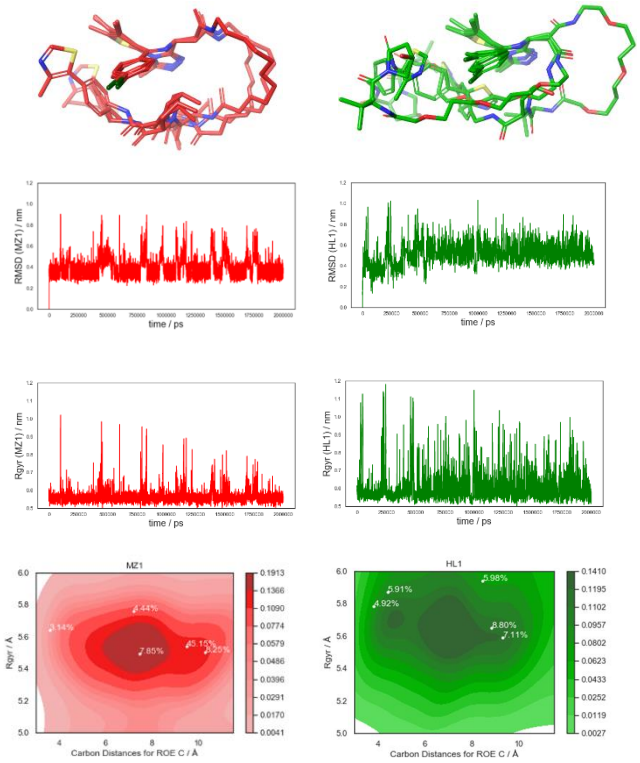

Figure 11. The top 3 major clustered geometries of hydrophilic **MZ1** (red, upper left) and **HL1** (green, upper right) sampled from unbiased MD simulation in water (2 us each by OPLS, alignment on JQ1 warhead). Different levels of conformational exchange were indicated by trajectory analysis based on RMSD and R_{gyr}. Those main clusters of each compound with corresponding population were labelled on the density map (**PC1**: carbon-carbon distances corresponding to rOe C; **PC2**: solute R_{gyr}).

The metastable binary complex of HL1CON with VHL

To further understand impacts of linker on binding and degradation behaviours, and particularly the experimentally observed hook-effect especially for **HL1CON**. we investigated conformations of PROTAC-bound binary complexes (i.e., with either VHL or BRD4:BD2) responsible for subsequent ternary complex formation.

Starting from the ternary complex of **MZ1** found by crystallography, we firstly replaced the BRD4:BD2 segment with explicit water (**Figure 12 a** left) and allowed this system to relax by unbiased simulation (2 replicates of 1 us at 300 K, OPLS). Two specific clusters, ***1A*** and ***1B***, were identified (**Figure 12 b**) comprising collapsed **MZ1** conformations where the **JQ1** warhead associates with the **VH032** warhead in the HIF binding pocket of VHL with a U-shape of the PEG3 linker, similar to the solution-state described before (**Figure 11** red). This collapse was also clear from the substantial reduction in both the ligand R_{gyr} and exposed surface area (ESA) on VHL during the simulation (**Figure 12 c** left). The MMPBSA scoring suggest these collapsed poses have binding energies comparable with the bioactive pose where the **JQ1** warhead is not in direct contact with VHL (**SI Section_17**). Hence, the **JQ1**-PEG3 moiety of **MZ1** does not appear to impair the residence of the **VH032** warhead on the VHL β-domain on simulated timescale. However, it does suggest that the **JQ1** warhead may be trapped on the VHL β-domain in this binary state, and thus kinetically disfavour any subsequent formation of the ternary complex by engaging BRD4:BD2, despite the end-state ternary complex being the thermodynamically preferred outcome with induced PPIs (**Figure 12 a** right). Interestingly, the **MZ1** bioactive conformation was observed as a transitory state after ~200 ns during the transition between collapsed conformations in one replicate of trajectory (**Figure 12 c** lower), providing a feasible pathway for **MZ1** to recruit BRD4:BD2 when bound with VHL and thus still allowing ternary complex formation. For those potent molecular glues (MG) generally with less or even no linker component, such modality should suffer less from entropic penalty of diverse non-bioactive conformations in the binary intermediate and hence have easier access to the productive ternary complex with robust protein-protein complementarity and ultra-high cooperativity.

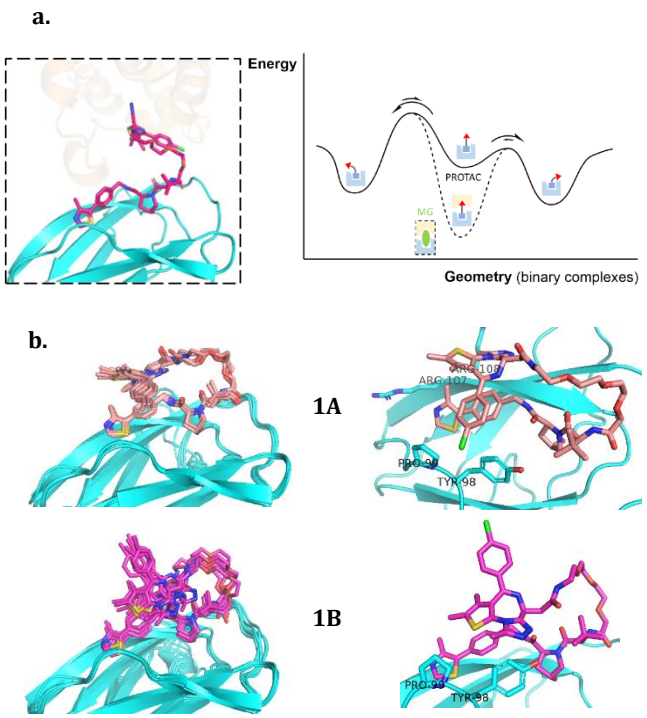

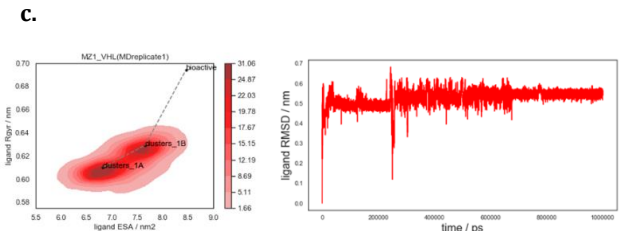

Figure 12. a. The unbiased simulations of **MZ1**-VHL binary complex system started from a bioactive pose, where BRD4:BD2 is eliminated from ternary complex crystallography (PDB: 5T35). **b.** Two clusters of collapse mode, **1A** and **1B**, were sampled and converged. The stable contact between JQ1 warhead and surface of VH032/VHL β-domain was observed. **c.** The simplified convergence pathway of one replicate starting from the bioactive state on landscape (density map - ***PC1***: ligand exposed surface area on VHL; ***PC2***: ligand Rgyr). The RMSD analysis of **MZ1** ligand trajectory suggested the bioactive conformation could be revisited after 200 ns during the transition among equilibrated collapse states.

Repeating this simulation for the **HL1CON-VHL** binary complex, by removing BRD4:BD2 from the **HL1CON**-bound ternary complex in previous modelling, afforded two distinct VHL-bound clusters respectively with good convergence (**Figure 13 a**). Unlike **MZ1**, the first major cluster ***A*** of **HL1CON** showed its **JQ1** warhead attaching between S1 and S4 sheets of VHL (**Figure 13 b** left, blue stick) whereas the second major cluster ***B*** showed the **JQ1** warhead of **HL1CON** shift away from the β-sheet and interact with the remote L1 and L3 loops of VHL (**Figure 13 b** right, blue stick). In contrast, corresponding simulations for the binary **HL1-VHL** complex failed to sample those states where the **JQ1** warhead collapsed onto VHL surface with significant residence time (**SI Section_17**).

To confirm the difference in VHL-bound behaviour between **HL1** and **HL1CON,** the two exposed β-gem-dimethyl substitutions were removed from **HL1CON-VHL** in either state ***A*** or state ***B*** poses to give the corresponding **HL1-VHL** poses (**Figure 13 b,** green stick), and 10 replicates of 200 ns unbiased simulation were performed starting from each collapsed state (**Figure 13 c**). Although state ***A*** was mostly retained for **HL1-VHL** (**Figure 13 b** left green stick), state ***B*** was lost in most trajectories. Again, this is in contrast with **HL1CON-VHL** where both states were generally retained following the same trials (**Figure 13 c**). This is also supported by the normal mode analysis for the **HL1CON** ligand trapped in state ***B*** with significantly lower entropy than all other simulation trials (**SI Section_17**). Only further heating (300 K to 420 K in 30 ns following each 200 ns equilibration) could accelerate the release of the **JQ1** warhead of PROTAC from all collapsed states on VHL surface.

These simulations with only the VHL receptor appeared to explain the unique low BRD4:BD2 cooperativity for **HL1CON** according to FP assay (α = 3) as well as its early onset of the hook-effect. This metastability of the collapsed **HL1CON-VHL** binary system would impair its subsequent binding and recruitment of BRD4:BD2 to ultimately form the productive ternary complex. However, it was unclear if such a phenomenon could be observed in any PROTAC binary complex with BRD4:BD2 as the more affinitive target.

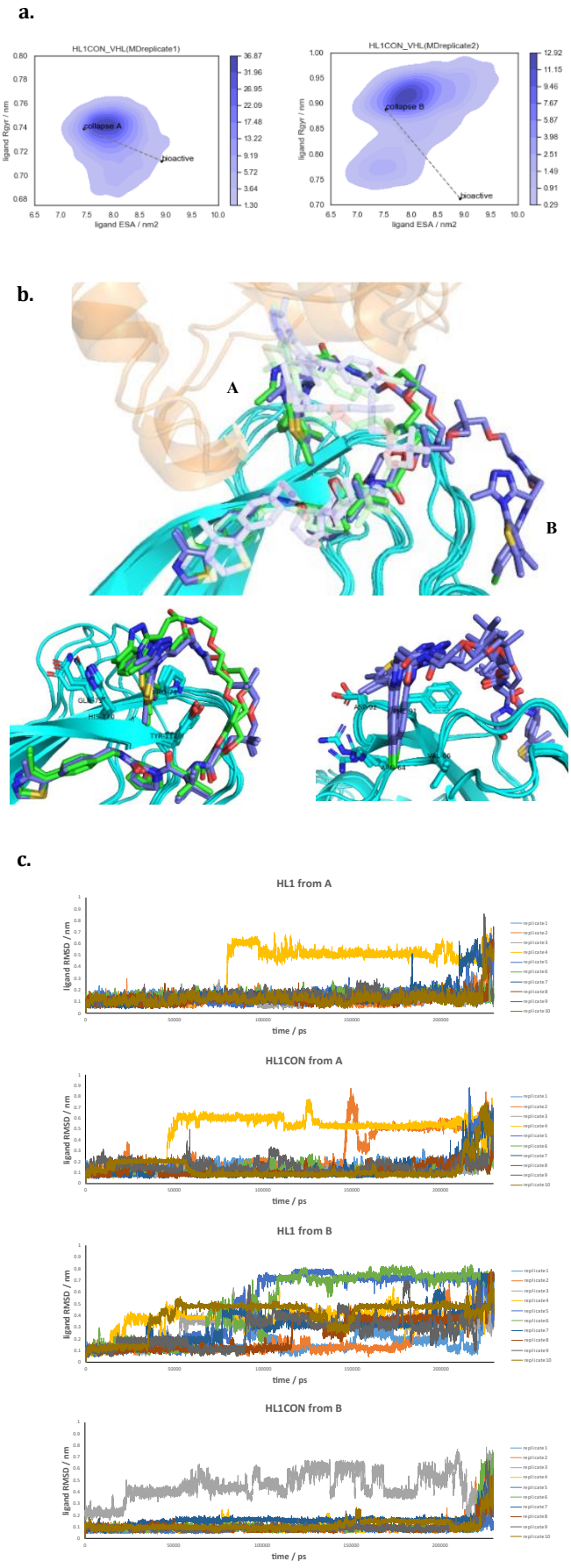

Figure 13 a. Density maps suggested the convergence of two replicates of 1 us unbiased simulation for **HL1CON-VHL** binary complex starting from the BRD4:BD2-eliminated bioactive pose, which led to afford two distinct collapse clusters, ***A*** and ***B.*** **b.** The collapse states ***A*** (left) could be adopted by both **HL1** and **HL1CON**, where both **JQ1** warheads were buried between S1 and S4 sheets. The state ***B*** (right) showed the **JQ1** warhead of **HL1CON** attaching on L1 and L3 loops of VHL. **c.** Further simulation trials (10*200 ns followed by 30 ns heating from 300 K to 420 K) starting from each collapse state on VHL indicated ***A*** as binary intermediates shared for both **HL1** and **HL1CON** while ***B*** is a unique metastable state for the linker constrained **HL1CON**.

The flexibility of VH032-based PROTACs in complex with BRD4:BD2

We then simulated the BRD4:BD2 binary complexes with just the **JQ1** warhead in explicit water. Due to the lack of an experimental co-crystal structure, homology alignment was applied to build the system of the BRD4:BD2-JQ1 complex based on analogous structural work on the BRD4:BD1-**JQ1** system from Bradner and co-workers.[11] Similar to their findings on BRD4:BD1, our unbiased simulation for BRD4:BD2 (2 replicates of 1 us) suggested that the **JQ1** inhibitor also stabilizes the fluctuation of both ZA and BC loops in this domain according to RMSF analysis (**Figure 14** and **SI Section_19**). Notably, those simulations in explicit water based on the OPLS force-field appeared to aggravate fluctuations of Bromodomain and aggregations with ligand compared to the AMBER/GAFF force-field, especially for the ZA loop not stabilized by VHL through PPIs. This phenomenon was not observed in our previous simulations for the VHL containing β-domain (**SI Section_18**). This aligns with observations in previous benchmark studies on force-field suitability.[56–58] Consequently, we adopted the AMBER/GAFF force-field for simulating all BRD4:BD2 binary complexes and found it gave a more satisfactory performance in this case.

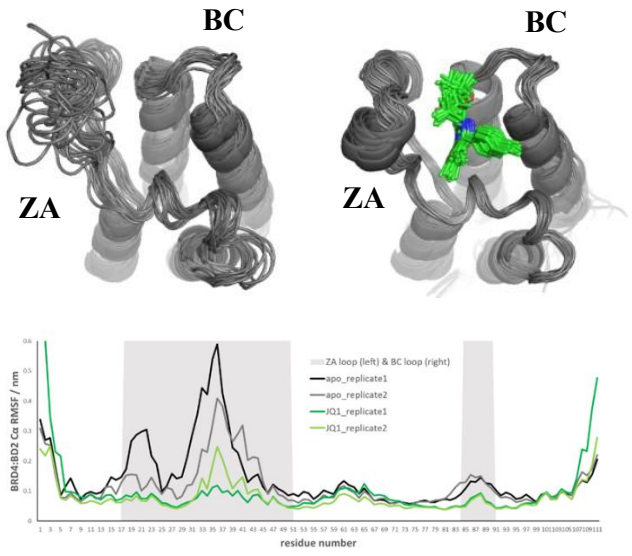

Figure 14. The simulations and RMSF analysis indicated both ZA and BC loops of BRD4:BD2 were stabilised by the **JQ1** ligand (AMBER/GAFF). Energy minimized clusters were shown for both *apo* (left) and JQ1 (right) bound systems (2 replicates of 1 us simulation for each system).

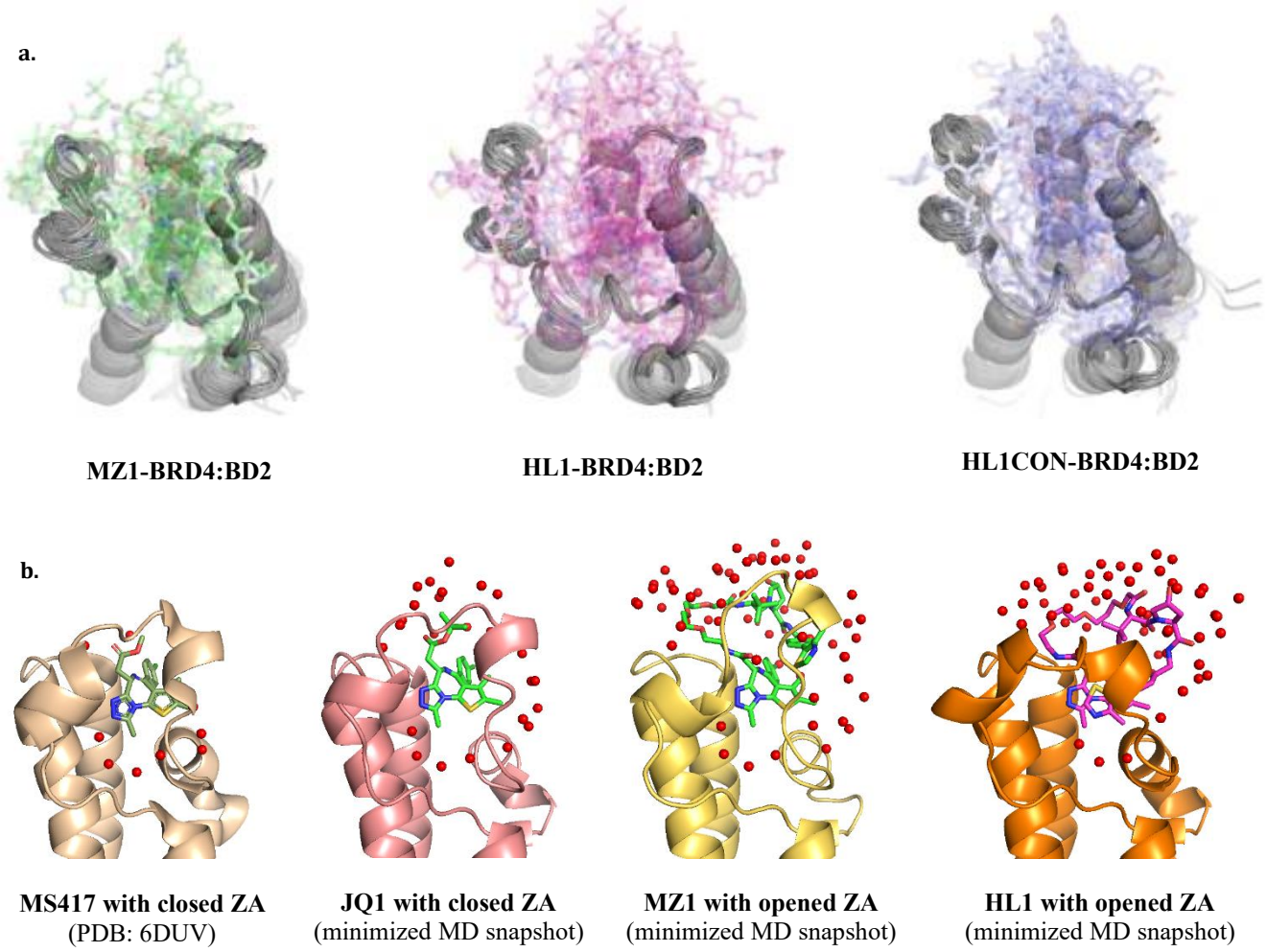

Figure 15 a. Diverse flexibilities of **VH032** warhead were observed from the JQ1 bound states of PROTAC **MZ1**, **HL1** and **HL1CON** (minimised ensembles as shown from left to right, 2 replicates of 1 us simulation for each system). **b.** The hydrophobic collapse of **HL1** and **HL1CON** respectively on BRD4:BD2 were also simulated that induce changes of ZA loop conformation and even conserved water distributions (AMBER/GAFF, TIP3P water models are shown within 5 Å of PROTAC ligand).

Following the above BRD4:BD2 simulation with the **JQ1** inhibitor, binary complexes with **MZ1**, **HL1** and **HL1CON** were simulated respectively, starting by removing VHL from their corresponding ternary complexes. As expected, trajectory analysis and minimized ensemble states suggested high flexibility of the **VH032** warhead under PROTAC-bound states of BRD4:BD2 in most cases (**Figure 15 a** & **SI Section_19**). However, the occasion where **VH032** collapsed into the **JQ1** binding pocket was still observed in two simulation pathways for **MZ1** and **HL1** with only their flexible and hydrophilic linkers exposed to solution (**Figure 15 b** shows minimized snapshots from corresponding trajectory). This led to the opening of ZA loop and changed the distribution of conserved waters in the pocket, which has not been observed in any crystallographic structures for Bromodomain. For the binary system of **HL1CON**-BRD4:BD2, no significant conformational change on BRD4:BD2 was observed in any pathway on simulated timescale (**SI Section_19**).

The experimental validation of unrestrained simulations for binary complexes in explicit solution was sought through chemical shift perturbations (CSP) measured using ^{1}H-^{15}N HMQC NMR spectroscopy for BRD4:BD2 titrated with soluble **MZ1** and **HL1** respectively.[60] The high similarity of the ^{1}H-^{15}N HMQC CSP fingerprints for BRD4:BD2 when 1:1 saturated with each PROTAC (**Figure 16 a** & **SI Section_20**), suggested that very similar binding modes to BRD4:BRD2 are adopted despite their linker difference. These were also found to be in line with reported HDX-MS data for BRD4:BD1 bound with those CRBN-based PROTACs,[24] suggesting comparable binary binding modes of such bivalent modality. Interestingly, large CSPs were identified not only in the region of presumably stabilized ZA loop but also around the BC loop and the helix bundle nearby. For **HL1** specifically (**Figure 16 b**), large CSPs of BRD4:BD2 were observed on S427, Y430 and A441, in line with bound snapshots from the MD ensemble bearing closed ZA loop. These support one hypothesis from simulations for diverse contacts between the unbound/free **VH032** warhead and the BRD4:BD2 receptor. Such solvent-exposed **VH032** flexibility may provide a prerequisite for the subsequent recruitment and adjustment with VHL E3-ligase. Different from the facile collapse of PROTACs on VHL, the flexibility of linker-**VH032** moiety beyond the **JQ1**-locked BRD4:BD2 is supposed to be critical as well for successful degradation events because the ternary complex could be adaptively formed prior to PROTAC saturation, collapse and hook on the less affinitive VHL E3-ligase in this case.

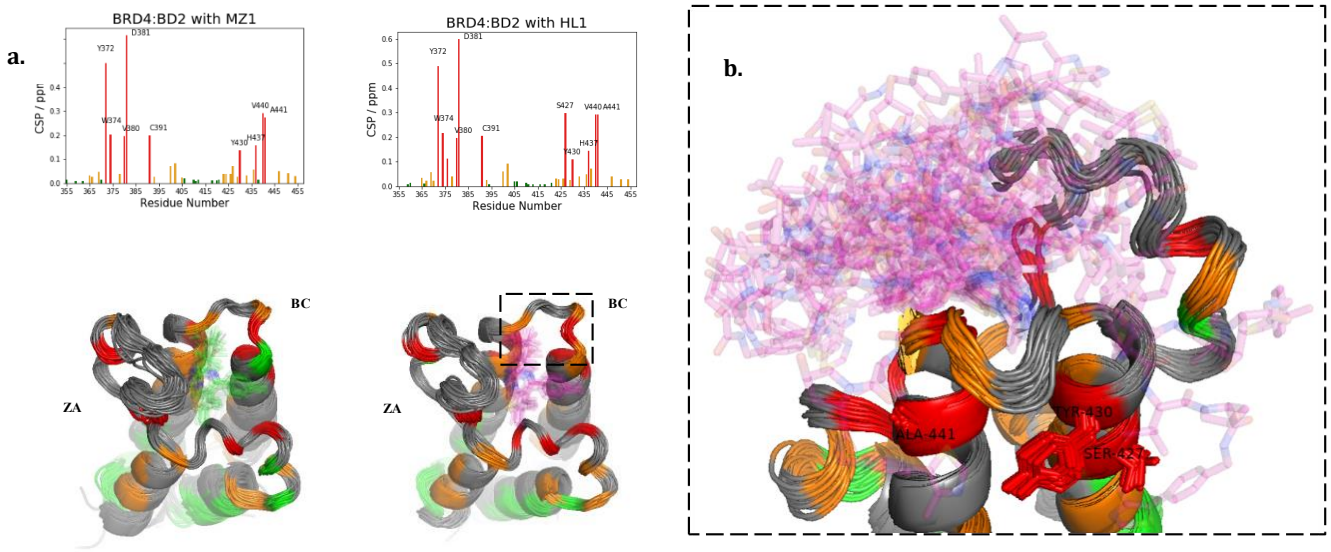

Figure 16 a. The perturbation of each chemical shift assigned for BRD4:BD2 under respective titration of **MZ1** (green) and **HL1** (pink) ([L]: [P] = 1, 1H-15N HMQC, 800 MHz). The map of CSP labelled on corresponding MD ensembles with closed ZA loop (CSP > 0.02 ppm in orange; CSP > 0.1 ppm in red; other assigned residues in green). The linker and VH032 warhead motifs were not shown in each ensemble. **b.** The large CSP of residues on the helix bundle near BC loop could be rationalised by contacts with flexible VH032 warhead of **HL1** according to the MD ensembles with closed ZA loop.

Summary

Herein, we applied a structure-based strategy and predictive computational modelling to modify the PEG3 linker in PROTAC **MZ1** to explore VHL-based BET degraders with high BRD4:BD2 cooperativity (**Figure 17**). The alternative PPG3 linker of **HL1** was designed to further stabilise productive ternary complexes originally formed by **MZ1** according to available crystal structure. Meanwhile, the pan-BET PROTAC **ARV771** was modelled to show the plasticity of ternary complex, where the BRD4:BD2 target is shifted to another position on VHL E3-ligase, and such a pose could allow broad degradation selectivity of the BET family. This work benefited from the utilization of a simple approach of multiple simulated annealing (MSA) in enhanced MD simulations, without any artificial biased potential along collective variable (CV) or expensive weighted ensemble (WE) / Markov-state Modelling (MSM),[63,64] to accelerate conformational exchange and identify rare conformational transitions for global energy minimizations when starting from a crystallographic geometry with high stability. Since small alteration of linker might be able to induce completely different pose of ternary complex, it again addresses the importance of physics-driven modelling and linker conformational analysis in the structure-based PROTAC optimizations.

To further stabilize ternary complexes for BRD4:BD2 selectivity and improve PROTAC physicochemical properties, we restrained conformations of the PPG3 linker with hydrophobic β-gem-dimethyl substitutions, leading to the design of **HL1CON**. The modelling on **HL1CON** suggested similar poses of the ternary complex could be formed, even though the ligand seemed to collapse with hydrophobic methyl groups added to the linker. The cellular degradation assays indicated contrary activities between the two PPG3 linked PROTACs, as **HL1** showed **MZ1**-comparable potent BET degradation with moderate BRD4 selectivity whereas **HL1CON** is also BRD4-selective but far less potent and suffered from earlier onset of the hook-effect. Further biophysical and DMPK assays revealed both PPG3-linked PROTACs have reduced binary and ternary binding affinities with VHL and BRD4:BD2 compared to **MZ1**, although the decay of **HL1** was minimal due to compensatory high cooperativity and good permeability. In contrast, neither high cooperativity nor permeability was observed for lipophilic **HL1CON** with poor solubility.

We found the high lipophilicity of **HL1CON** presumably caused its retention in bi-directional caco-2 assay, suggested by low recovery ratios. Moreover, extra methyl substitutions on the PPG3 linker lead **HL1CON** to have intensive collapse in DMSO and aqueous mixtures according to QM/DFT-level computational modelling and experimental rOe data. This is assumed to bring a significant entropic penalty of de-solvation for **HL1CON** against the binding process either with VHL or with BRD4:BD2, whereas both hydrophilic **MZ1** and **HL1** could adopt more 'chameleonic' conformations including various U-shaped minima in aqueous solution.

Furthermore, comprehensive simulations suggested a unique metastable equilibrium for **HL1CON**-VHL binary systems where the **JQ1** warhead is stuck between the L1 and L3 loops under linker constraint. The state is quite different from the bioactive conformation required for the subsequent ternary complex formation and suggests an origin for its 'hook effect' observed experimentally at relatively higher concentrations. In contrast, all PROTAC binary systems with BRD4:BD2 demonstrated high flexibilities of **VH032**, even though such VHL warhead could tangle with opened ZA loop in some states according to extensive simulations.

In summary, this research expands our understanding of the potential risks and benefits of conformational control, linker rigidification and hydrophobicity in PROTAC drug discovery for targeted protein degradation (TPD). Although constraining PROTAC linker freedom has been widely considered as an efficient strategy to improve the permeability through 'hydrophobic collapse' and facilitate the final formation of ternary complex regarding entropy in some systems,[61,62,63] this study highlights the importance of balancing this with considera-

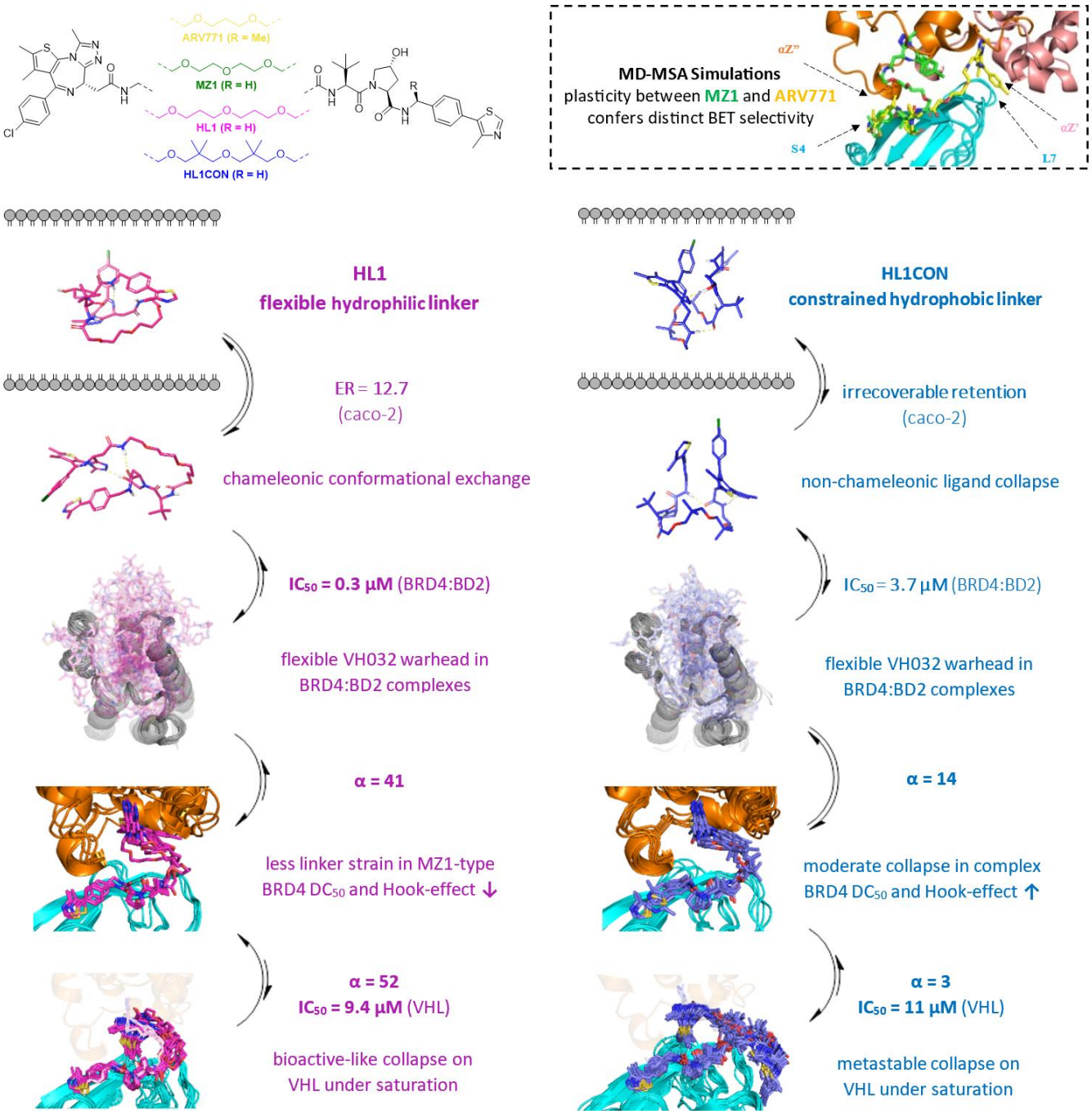

Figure 17. The summary of ternary complex plasticity between **MZ1** and **ARV771** as well as the conformation-activity relationships for **HL1** and **HL1CON**, showing different degradation behaviours by comparison in each step.

tions of NMR solution structures, intermediates' dynamics and accessible conformations for degrader ligands in all states.

ASSOCIATED CONTENT

Supporting Information. The Supporting Information including computational procedures for conformational analysis and experimental procedures for compound synthesis, cellular and biophysical assays. All supplementary figures, schemes, charts, tables, and NMR spectra are also included. All modelling (Gaussian and ORCA files of DFT calculation, Gromacs files of MD trajectory with force-field parameters) and NMR (FID) row data are available upon reasonable request.

AUTHOR INFORMATION

Corresponding Author

*craig.butts@bristol.ac.uk

*v.aggarwal@bristol.ac.uk

*a.ciulli@dundee.ac.uk

Present Addresses

†Present address: Amphista Therapeutics Ltd, Granta Park, Cambridge, CB21 6GQ, United Kingdom.

Author Contributions

Hao Lan designed PROTACs, conducted computational modelling, NMR experiment and chemical synthesis activities along with data analysis and some biophysical experiments. Oliver Hsia led the activities of cellular and biophysical experiments and undertook the majority of that work. Mark Nakasone and Hao Lan prepared ^{15}N-labelled BRD4:BD2 and conducted protein NMR assays. Andre Wijaya and Hao Lan conducted FP assays. The manuscript was written through contributions of all authors. All authors have given approval to the final version of the manuscript.

Funding Sources

H.L. thanks the Bristol Chemical Synthesis Centre for Doctoral Training, funded by EPSRC (EP/L015366/1) and the University of Bristol, for a Ph.D. studentship. The work of the Ciulli laboratory on targeting E3 ligases and TPD has received funding from the European Research Council (ERC) under the European Union's Seventh Framework Programme (FP7/2007-2013) as a Starting Grant to A.C. (grant agreement ERC-2012-StG-311460 DrugE3CRLs), and the Innovative Medicines Initiative 2 (IMI2) Joint Undertaking under grant agreement no. 875510 (EUbOPEN project). The IMI2 Joint Undertaking receives support from the European Union's Horizon 2020 research and innovation program, European Federation of Pharmaceutical Industries and Associations (EFPIA) companies, and associated partners KTH, OICR, Diamond, and McGill.

Notes

The Ciulli laboratory receives or has received sponsored research support from Almirall, Amgen, Amphista Therapeutics, Boehringer Ingelheim, Eisai, Merck KGaA, Nurix Therapeutics, Ono Pharmaceutical and Tocris-Biotechne. A.C. is a scientific founder, shareholder, and advisor of Amphista Therapeutics, a company that is developing targeted protein degradation therapeutic platforms.

ACKNOWLEDGMENT

H.L. thanks Prof. C. Redfield and Prof. T. Claridge (University of Oxford) for the assistance of 950MHz NMR experiments, Dr. C. Williams (UoB) for the assistance of 600MHz NMR experiments, Dr. S. Oliveira (UoB) for the discussion of protein simulations and Dr. S. Aiken (UoB) for the HPLC purification of PROTACs. All molecular modelling works were carried out using the computational facilities of the Advanced Computing Research Centre, University of Bristol. H.L. also thanks Dr. A. Bond for generous donations of BRD4:BD2 and VHL proteins. H.L. and M.N. acknowledge EPSRC grant (EP/R030065/1) for access to the 800 MHz NMR with assistance from Dr. Juraj Bella and Prof. Dusan Uhrin (University of Edinburgh).

ABBREVIATIONS

PROTAC@, proteolysis targeting chimeras (a brand registered by Arvinas); TPD, targeted protein degradation; POI, protein of interest; VHL, Von Hippel-Lindau; BET, Bromo and Extra-Terminal domain; MD-MSA, molecular dynamics simulation with multiple simulated annealing; HDX-MS; hydrogen/deuterium exchange mass spectrometry; CSP, chemical shift perturbation; IMHBs, intramolecular hydrogen bonds.

REFERENCES

(1) Békés, M.; Langley, D. R.; Crews, C. M. PROTAC Targeted Protein Degraders: The Past Is Prologue. Nat Rev Drug Discov 2022, 21 (3), 181-200.

(2) Tinworth, C. P.; Lithgow, H.; Churcher, I. Small Molecule-Mediated Protein Knockdown as a New Approach to Drug Discovery. Medchemcomm 2016, 7 (12), 2206–2216.

(3) Bondeson, D. P.; Mares, A.; D Smith, I. E.; Ko, E.; Campos, S.; Miah, A. H.; Mulholland, K. E.; Routly, N.; Buckley, D. L.; Gustafson, J. L.; Zinn, N.; Grandi, P.; Shimamura, S.; Bergamini, G.; Faelth-Savitski, M.; Bantscheff, M.; Cox, C.; Gordon, D. A.; Willard, R. R.; Flanagan, J. J.; Casillas, L. N.; Votta, B. J.; den Besten, W.; Famm, K.; Kruidenier, L.; Carter, P. S.; Harling, J. D.; Churcher, I.; Crews, C. M. Catalytic in Vivo Protein Knockdown by Small-Molecule PROTACs. Nat Chem Biol 2015, 11, 611-617.

(4) Diehl, C. J.; Ciulli, A. Discovery of Small Molecule Ligands for the von Hippel-Lindau (VHL) E3 Ligase and Their Use as Inhibitors and PROTAC Degraders. Chem Soc Rev 2022, 51(19), 8143-8408.

(5) Zengerle, M.; Chan, K. H.; Ciulli, A. Selective Small Molecule Induced Degradation of the BET Bromodomain Protein BRD4. ACS Chem Biol 2015, 10 (8), 1770–1777.

(6) Chan, K. H.; Zengerle, M.; Testa, A.; Ciulli, A. Impact of Target Warhead and Linkage Vector on Inducing Protein Degradation: Comparison of Bromodomain and Extra-Terminal (BET) Degraders Derived from Triazolodiazepine (JQ1) and Tetrahydroquinoline (I-BET726) BET Inhibitor Scaffolds. J Med Chem 2018, 61 (2), 504–513.

(7) Raina, K.; Lu, J.; Qian, Y.; Altieri, M.; Gordon, D.; Rossi, A. M. K.; Wang, J.; Chen, X.; Dong, H.; Siu, K.; Winkler, J. D.; Crew, A. P.; Crews, C. M.; Coleman, K. G. PROTAC-Induced BET Protein Degradation as a Therapy for Castration-Resistant Prostate Cancer. Proc Natl Acad Sci U S A 2016, 113 (26), 7124–7129.

(8) Galdeano, C.; Gadd, M. S.; Soares, P.; Scaffidi, S.; Van Molle, I.; Birced, I.; Hewitt, S.; Dias, D. M.; Ciulli, A. Structure-Guided Design and Optimisation of Small Molecules Targeting the Protein-Protein Interaction between the von Hippel-Lindau (VHL) E3 Ubiquitin Ligase and the Hypoxia Inducible Factor (HIF) Alpha Subunit with in Vitro Nanomolar Affinities. J Med Chem 2014, 57 (20), 8657–8663.

(9) Winter, G. E.; Buckley, D. L.; Paulk, J.; Roberts, J. M.; Souza, A.; Dhe-Paganon, S.; Bradner, J. E. Phthalimide Conjugation as a Strategy for in Vivo Target Protein Degradation. Science 2015, 348 (6241), 1376–1381.

(10) Nowak, R. P.; Deangelo, S. L.; Buckley, D.; He, Z.; Donovan, K. A.; An, J.; Safaee, N.; Jedrychowski, M. P.; Ponthier, C. M.; Ishoey, M.; Zhang, T.; Mancias, J. D.; Gray, N. S.; Bradner, J. E.; Fischer, E. S. Plasticity in Binding Confers Selectivity in Ligand-Induced Protein Degradation Article. Nat Chem Biol 2018, 14 (7), 706–714.

(11) Filippakopoulos, P.; Qi, J.; Picaud, S.; Shen, Y.; Smith, W. B.; Fedorov, O.; Morse, E. M.; Keates, T.; Hickman, T. T.; Felletar, I.; Philpott, M.; Munro, S.; McKeown, M. R.; Wang, Y.; Christie, A. L.; West, N.; Cameron, M. J.; Schwartz, B.; Heightman, T. D.; La Thangue, N.; French, C. A.; Wiest, O.; Kung, A. L.; Knapp, S.; Bradner, J. E. Selective Inhibition of BET Bromodomains. Nature 2010, 468 (7327), 1067–1073.

(12) Winter, G. E.; Mayer, A.; Buckley, D. L.; Erb, M. A.; Roderick, J. E.; Vittori, S.; Reyes, J. M.; di Iulio, J.; Souza, A.; Ott, C. J.; Roberts, J. M.; Zeid, R.; Scott, T. G.; Paulk, J.; Lachance, K.; Olson, C. M.; Dastjerdi, S.; Bauer, S.; Lin, C. Y.; Gray, N. S.; Kelliher, M. A.; Churchman, L. S.; Bradner, J. E. BET Bromodomain Proteins Function as Master Transcription Elongation Factors Independent of CDK9 Recruitment. Mol Cell 2017, 67 (1), 5-18.e19.

(13) Gadd, M. S.; Testa, A.; Lucas, X.; Chan, K. H.; Chen, W.; Lamont, D. J.; Zengerle, M.; Ciulli, A. Structural Basis of PROTAC Co-operative Recognition for Selective Protein Degradation. Nat Chem Biol 2017, 13 (5), 514–521.

(14) Roy, M. J.; Winkler, S.; Hughes, S. J.; Whitworth, C.; Galant, M.; Farnaby, W.; Rumpel, K.; Ciulli, A. SPR-Measured Dissociation Kinetics of PROTAC Ternary Complexes Influence Tar-get Degradation Rate. ACS Chem Biol 2019, 14 (3), 361–368.

(15) Pfaff, P.; Samarasinghe, K. T. G.; Crews, C. M.; Carreira, E. M. Reversible Spatiotemporal Control of Induced Protein Degradation by Bistable PhotoPROTACs. ACS Cent Sci 2019, 5 (10), 1682–1690.

(16) Bemis, T. A.; La Clair, J. J.; Burkart, M. D. Unraveling the Role of Linker Design in Proteolysis Targeting Chimeras. J Med Chem 2021, 64 (12), 8042-8052.

(17) Testa, A.; Hughes, S. J.; Lucas, X.; Wright, J. E.; Ciulli, A. Structure-Based Design of a Macrocyclic PROTAC. Angewandte Chemie - International Edition 2020, 59 (4), 1727–1734.

(18) Testa, A.; Lucas, X.; Castro, G. V.; Chan, K. H.; Wright, J. E.; Runcie, A. C.; Gadd, M. S.; Harrison, W. T. A.; Ko, E. J.; Fletcher, D.; Ciulli, A. 3-Fluoro-4-Hydroxyprolines: Synthesis, Con-formational Analysis, and Stereoselective Recognition by the VHL E3 Ubiquitin Ligase for Targeted Protein Degradation. J Am Chem Soc 2018, 140 (29), 9299–9313.

(19) Klein, V. G.; Bond, A. G.; Craigon, C.; Lokey, R. S.; Ciulli, A. Amide-to-Ester Substitution as a Strategy for Optimising PROTAC Permeability and Cellular Activity. J Med Chem 2021, 64 (24), 18082–18101.

(20) Imaide, S.; Riching, K. M.; Makukhin, N.; Vetma, V.; Whitworth, C.; Hughes, S. J.; Trainor, N.; Mahan, S. D.; Murphy, N.; Cowan, A. D.; Chan, K. H.; Craigon, C.; Testa, A.; Maniaci, C.; Urh, M.; Daniels, D. L.; Ciulli, A. Trivalent PROTACs Enhance Protein Degradation via Combined Avidity and Cooperativity. Nat Chem Biol 2021, 17 (11), 1157–1167.

(21) Huang, Y.; Yokoe, H.; Kaiho-Soma, A.; Takahashi, K.; Hira-sawa, Y.; Morita, H.; Ohtake, F.; Kanoh, N. Design, Synthesis, and Evaluation of Trivalent PROTACs Having a Functionalisation Site with Controlled Orientation. Bioconjug Chem 2022, 33 (1), 142–151.

(22) Weerakoon, D.; Carbajo, R. J.; De Maria, L.; Tyrchan, C.; Zhao, H. Impact of PROTAC Linker Plasticity on the Solution Conformations and Dissociation of the Ternary Complex. J Chem Inf Model 2022, 62 (2), 340–349.

(23) Schiemer, J.; Horst, R.; Meng, Y.; Montgomery, J. I.; Xu, Y.; Feng, X.; Borzilleri, K.; Uccello, D. P.; Leverett, C.; Brown, S.; Che, Y.; Brown, M. F.; Hayward, M. M.; Gilbert, A. M.; Noe, M. C.; Calabrese, M. F. Snapshots and Ensembles of BTK and CIAP1 Protein Degrader Ternary Complexes. Nat Chem Biol 2021, 17 (2), 152–160.

(24) Eron, S. J.; Huang, H.; Agafonov, R. V.; Fitzgerald, M. E.; Patel, J.; Michael, R. E.; Lee, T. D.; Hart, A. A.; Shaulsky, J.; Nasveschuk, C. G.; Phillips, A. J.; Fisher, S. L.; Good, A. Structural Characterisation of Degrader-Induced Ternary Complexes Using Hydrogen-Deuterium Exchange Mass Spectrometry and Computational Modelling: Implications for Structure-Based Design. ACS Chem Biol 2021, 16 (11), 2228–2243.

(25) Li, W.; Zhang, J.; Guo, L.; Wang, Q. Importance of Three-Body Problems and Protein-Protein Interactions in Proteolysis-Targeting Chimera Modelling: Insights from Molecular Dynamics Simulations. J Chem Inf Model 2022, 62 (3), 523–532.

(26) Liao, J.; Nie, X.; UnartaI, C.; Ericksen, S. S.; Tang, W. In Silico Modeling and Scoring of PROTAC-Mediated Ternary Complex Poses. J Med Chem 2022, 65 (8), 6116-6132.

(27) Dragovich, P. S.; Pillow, T. H.; Blake, R. A.; Sadowsky, J. D.; Adaligil, E.; Adhikari, P.; Chen, J.; Corr, N.; Dela Cruz-Chuh, J.; Del Rosario, G.; Fullerton, A.; Hartman, S. J.; Jiang, F.; Kauf-man, S.; Kleinheinz, T.; Kozak, K. R.; Liu, L.; Lu, Y.; Mulvihill, M. M.; Murray, J. M.; O'Donohue, A.; Rowntree, R. K.; Sawyer, W. S.; Staben, L. R.; Wai, J.; Wang, J.; Wei, B.; Wei, W.; Xu, Z.; Yao, H.; Yu, S. F.; Zhang, D.; Zhang, H.; Zhang, S.; Zhao, Y.; Zhou, H.; Zhu, X. Antibody-Mediated Delivery of Chimeric BRD4 Degraders. Part 2: Improvement of in Vitro Antiproliferation Activity and in Vivo Antitumor Efficacy. J Med Chem 2021, 64 (5), 2576–2607.

(28) Krieger, J.; Sorrell, F. J.; Wegener, A. A.; Leuthner, B.; Machrouhi-Porcher, F.; Hecht, M.; Leibrock, E. M.; Müller, J. E.; Eisert, J.; Hartung, I. V.; Schlesiger, S. Systematic Potency and Property Assessment of VHL Ligands and Implications on PROTAC Design. ChemMedChem 2023, 18, e202200615.

(29) Drummond, M. L.; Williams, C. I. In Silico Modelling of PROTAC-Mediated Ternary Complexes: Validation and Application. J Chem Inf Model 2019, 59 (4), 1634–1644.

(30) Drummond, M. L.; Henry, A.; Li, H.; Williams, C. I. Improved Accuracy for Modelling PROTAC-Mediated Ternary Complex Formation and Targeted Protein Degradation via New in Silico Methodologies. J Chem Inf Model 2020, 60 (10), 5234–5254.

(31) Bai, N.; Miller, S. A.; Andrianov, G. V.; Yates, M.; Kirubakaran, P.; Karanicolas, J. Rationalising PROTAC-Mediated Ternary Complex Formation Using Rosetta. J Chem Inf Model 2021, 61 (3), 1368–1382.

(32) Zaidman, D.; Prilusky, J.; London, N. ProsetTac: Rosetta Based Modelling of PROTAC Mediated Ternary Complexes. J Chem Inf Model 2020, 60 (10), 4894–4903.

(33) Weng, G.; Li, D.; Kang, Y.; Hou, T. Integrative Modelling of PROTAC-Mediated Ternary Complexes. J Med Chem 2021, 64 (21), 16271–16281.

(34) Ignatov, M.; Jindal, A.; Kotelnikov, S.; Beglov, D.; Posternak, G.; Tang, X.; Maisonneuve, P.; Poda, G.; Batey, R. A.; Sicheri, F.; Whitty, A.; Tonge, P. J.; Vajda, S.; Kozakov, D. High Accuracy Prediction of PROTAC Complex Structures. J Am Chem Soc 2023, 145 (13), 7123-7135.

(35) Hanzl, A.; Casement, R.; Imrichova, H.; Hughes, S. J.; Barone, E.; Testa, A.; Bauer, S.; Wright, J.; Brand, M.; Ciulli, A.; Winter, G. E. Functional E3 Ligase Hotspots and Resistance Mechanisms to Small-Molecule Degraders. Nat Chem Biol 2022, 19 (3), 323-333.

(36) Smith, G. D.; Jaffe, R. L.; Yoon, D. Y. Conformational Characteristics of 1,3-Dimethoxypropane and Poly(Oxytrimethylene) Based upon Ab Initio Electronic Structure Calculations. Journal of Physical Chemistry 1996, 100 (32), 13439–13446.

(37) Bultinck, P.; Van Alsenoy, C.; Goeminne, A. Theoretical Conformational Analysis of 1,3-Dimethoxypropane and 14-Crown-4: Importance of Stabilising Intramolecular Interactions. Journal of Physical Chemistry A 2001, 105 (40), 9203–9210.

(38) Gil, S.; Espinosa, J. F.; Parella, T. IPAP-HSQMBC: Measurement of Long-Range Heteronuclear Coupling Constants from Spin-State Selective Multiplets. Journal of Magnetic Resonance 2010, 207 (2), 312–321.

(39) Dickson, C. L.; Blundell, C. D.; Butts, C. P.; Felton, A.; Jeffreys, A.; Takacs, Z. Accurate Measurement of Long-Range Proton-Carbon Scalar Coupling Constants. Analyst 2017, 142 (4), 621–633.

(40) Wu, J.; Lorenzo, P.; Zhong, S.; Ali, M.; Butts, C. P.; Myers, E. L.; Aggarwal, V. K. Synergy of Synthesis, Computation and NMR Reveals Correct Baulamycin Structures. Nature 2017, 547 (7664), 436–440.

(41) Burns, M.; Essafi, S.; Bame, J. R.; Bull, S. P.; Webster, M. P.; Balieu, S.; Dale, J. W.; Butts, C. P.; Harvey, J. N.; Aggarwal, V. K. Assembly-Line Synthesis of Organic Molecules with Tailored Shapes. Nature 2014, 513 (7517), 183–188.

(42) Guo, L.; Dutton, O. J.; Kucukdisli, M.; Davy, M.; Wagnières, O.; Butts, C. P.; Myers, E. L.; Aggarwal, V. K. Conformationally Controlled Linear and Helical Hydrocarbons Bearing Extended Side Chains. J Am Chem Soc 2021, 143 (40), 16682–16692.

(43) Pradeilles, J. A.; Zhong, S.; Baglyas, M.; Tarczay, G.; Butts, C. P.; Myers, E. L.; Aggarwal, V. K. Odd–Even Alternations in Helical Propensity of a Homologous Series of Hydrocarbons. Nat Chem 2020, 12, 475-480.

(44) Douglass, E. F.; Miller, C. J.; Sparer, G.; Shapiro, H.; Spiegel, D. A. A Comprehensive Mathematical Model for Three-Body Binding Equilibria. J Am Chem Soc 2013, 135 (16), 6092–6099.

(45) Cecchini, C.; Pannilunghi, S.; Tardy, S.; Scapozza, L. From Conception to Development: Investigating PROTACs Features for Improved Cell Permeability and Successful Protein Degradation. Frontiers in Chemistry 2021, 9.

(46) Roberts, J. M.; Bradner, J. E. A Bead-Based Proximity Assay for BRD4 Ligand Discovery. Curr Protoc Chem Biol 2015, 7 (4), 263–278.

(47) Scott, D. E.; Rooney, T. P. C.; Bayle, E. D.; Mirza, T.; Willems, H. M. G.; Clarke, J. H.; Andrews, S. P.; Skidmore, J. Systematic Investigation of the Permeability of Androgen Receptor PROTACs. ACS Med Chem Lett 2020, 11 (8), 1539–1547.

(48) Klein, V. G.; Townsend, C. E.; Testa, A.; Zengerle, M.; Maniaci, C.; Hughes, S. J.; Chan, K. H.; Ciulli, A.; Lokey, R. S. Understanding and Improving the Membrane Permeability of VH032-Based PROTACs. ACS Med Chem Lett 2020, 11 (9), 1732–1738.

(49) Donovan, D. H. O.; Fusco, C. De; Kuhnke, L.; Reichel, A. Trends in Molecular Properties, Bioavailability, and Permeability across the Bayer Compound Collection. 2023, 66 (4), 2347-2360.

(50) Atilaw, Y.; Poongavanam, V.; Svensson Nilsson, C.; Nguyen, D.; Giese, A.; Meibom, D.; Erdelyi, M.; Kihlberg, J. Solution Conformations Shed Light on PROTAC Cell Permeability. ACS Med Chem Lett 2021, 12 (1), 107–114.

(51) Poongavanam, V.; Atilaw, Y.; Siegel, S.; Giese, A.; Lehmann, L.; Meibom, D.; Erdelyi, M.; Kihlberg, J. Linker-Dependent Folding Rationalises PROTAC Cell Permeability. J Med Chem 2022, 65 (19), 13029–13040.

(52) Butts, C. P.; Jones, C. R.; Song, Z.; Simpson, T. J. Accurate NOE-Distance Determination Enables the Stereochemical Assignment of a Flexible Molecule – Arugosin C. Chemical Communications 2012, 48 (72), 9023–9025.

(53) Butts, C. P.; Jones, C. R.; Harvey, J. N. High Precision NOEs as a Probe for Low Level Conformers—a Second Conformation of Strychnine. Chemical Communications 2011, 47 (4), 1193–1195.

(54) Butts, C. P.; Jones, C. R.; Towers, E. C.; Flynn, J. L.; Appleby, L.; Barron, N. J. Interproton Distance Determinations by NOE - Surprising Accuracy and Precision in a Rigid Organic Molecule. Org Biomol Chem 2011, 9 (1), 177–184.

(55) Tang, R.; Wang, Z.; Xiang, S.; Wang, L.; Yu, Y.; Wang, Q.; Deng, Q.; Hou, T.; Sun, H. Uncovering the Kinetic Characteristics and Degradation Preference of PROTAC Systems with Advanced Theoretical Analyses. JACS Au, 2023, 3 (6), 1775-1789.

(56) Matthes, D.; De Groot, B. L. Secondary Structure Propensities in Peptide Folding Simulations: A Systematic Comparison of Molecular Mechanics Interaction Schemes. Biophys J 2009, 97 (2), 599–608.

(57) Smith, M. D.; Rao, J. S.; Segelken, E.; Cruz, L. Force-Field Induced Bias in the Structure of Aβ21-30: A Comparison of OPLS, AMBER, CHARMM, and GROMOS Force Fields. J Chem Inf Model 2015, 55 (12), 2587–2595.

(58) Carballo-Pacheco, M.; Ismail, A. E.; Strodel, B. On the Applicability of Force Fields to Study the Aggregation of Amyloidogenic Peptides Using Molecular Dynamics Simulations. J Chem Theory Comput 2018, 14 (11), 6063–6075.

(59) Zhang, G.; Liu, R.; Zhong, Y.; Plotnikov, A. N.; Zhang, W.; Zeng, L.; Rusinova, E.; Gerona-Nevarro, G.; Moshkina, N.; Joshua, J.; Chuang, P. Y.; Ohlmeyer, M.; He, J. C.; Zhou, M. M. Down-Regulation of NF-KB Transcriptional Activity in HIV-Associated Kidney Disease by BRD4 Inhibition. Journal of Biological Chemistry 2012, 287 (34), 28840–28851.

(60) Liu, Y.; Wang, X.; Zhang, J.; Huang, H.; Ding, B.; Wu, J.; Shi, Y. Structural Basis and Binding Properties of the Second Bromodomain of Brd4 with Acetylated Histone Tails. Biochemistry 2008, 47 (24), 6403–6417.

(61) Kofink, C.; Trainor, N.; Mair, B.; Wöhrle, S.; Wurm, M.; Mischerikow, N.; Roy, M. J.; Bader, G.; Greb, P.; Garavel, G.; Diers, E.; McLennan, R.; Whitworth, C.; Vetma, V.; Rumpel, K.; Scharnweber, M.; Fuchs, J. E.; Gerstberger, T.; Cui, Y.; Gremel, G.; Chetta, P.; Hopf, S.; Budano, N.; Rinnenthal, J.; Gmaschitz, G.; Mayer, M.; Koegl, M.; Ciulli, A.; Weinstabl, H.; Farnaby, W. A Selective and Orally Bioavailable VHL-Recruiting PROTAC Achieves SMARCA2 Degradation in Vivo. Nat Commun 2022, 13 (1), 1–15.

(62) Bashore, F. M.; Foley, C. A.; Ong, H. W.; Rectenwald, J. M.; Hanley, R. P.; Norris-Drouin, J. L.; Cholensky, S. H.; Mills, C. A.; Pearce, K. H.; Herring, L. E.; Kireev, D.; Frye, S. V.; James, L. I. PROTAC Linkerology Leads to an Optimised Bivalent Chemical Degrader of Polycomb Repressive Complex 2 (PRC2) Components. ACS Chemical Biology, 2023, 18 (3), 494-507.

(63) Dixon, T.; MacPherson, D.; Mostofian, B.; Dauzhenka, T.; Lotz, S.; McGee, D.; Shechter, S.; Shrestha, U. R.; Wiewiora, R.; McDargh, Z. A.; et al. Predicting the structural basis of targeted protein degradation by integrating molecular dynamics simulations with structural mass spectrometry. Nat. Commun. 2022,13, 588

(64) Mostofian, B.; Martin, H.; Razavi, A.; Patel, S.; Allen, B.; Sherman, W.; Izaguirre, J. A. Targeted Protein Degradation: Advances, Challenges, and Prospects for Computational Methods. J. Chem. Inf. Model. 2023, 63, 17, 5408–543

(65) Dewis, L. I.; Rudrakshula, M.; Williams, C.; Chiarparin, E.; Myers, E. L.; Butts, C. P.; Aggarwal, V. K. Conformationally Controlled sp^3-Hydrocarbon-Based α-Helix Mimetics. Angewandte Chemie - International Edition 2023, 62, e202301209.